ACS OMEGA

Open Access

http://pubs.acs.org/journal/acsodf

Article

Carbon Nanotube-Based Segregated Thermoplastic Nanocomposites Structured via Electromagnetic Melt Processing

Madara Mohoppu, Utsab Ayan, Jacob Schwartz, Ahmed Al-Ostaz, Mine G. Ucak-Astarlioglu, and Byron S. Villacorta*

Cite This: *ACS Omega* 2024, 9, 48546−48562

Read Online

ACCESS | Metrics & More | Article Recommendations | Supporting Information

ABSTRACT: A cutting-edge method that uses electromagnetic (EM) energy for the melt processing of thermoplastic polymer nanocomposites (TPNCs) is reported. The properties and microstructures of TPNCs produced via the proposed EM-processing method and TPNCs via conventional heat processing are contrasted. The EM-processed TPNCs prepared with EM-susceptible carbon nanotubes (CNTs) exhibited a significant enhancement in transport and mechanical properties, outperforming the conventionally processed TPNCs. Thus, the EM-processed TPNCs demonstrated an ultralow electrical percolation threshold (∼0.09 vol %) and a remarkable increase in volume electrical conductivity of 8 orders of magnitude (i.e., 1.1×10^{-5} S/m) at only 1.0 wt % CNT loading, compared to their hot-pressed counterparts. This highlights the superior network formation, level of segregation, and structuring enabled by EM processing. Differential scanning calorimetry (DSC) and X-ray diffraction (XRD) revealed that EM-processed TPNCs exhibited higher crystallinity (∼9% higher) and a predominantly α crystal phase compared to the hot-pressed TPNCs. Microstructural inspection by electron microscopy disclosed that EM processing led to segregated but interconnected multiscale networks of a thin and well-defined CNT interphase that encompassed from the nanoscale of the CNTs to the macroscopic scale of TPNCs. In contrast, conventional processing developed a more diffused CNT interphase with less interconnectivity. The EM-processed TPNCs developed a statistically higher stiffness (+20%) and in certain cases, even better strength (+10%) than the hot-pressed TPNCs. However, the EM-processed TPNCs displayed significantly lower ductility, owing to their higher crystallinity, more brittle crystal α phase, and the potential formation of microvoids in the bulk of the TPNCs inherent to the unoptimized EM processing. This work provides an understanding of an alternative and unconventional processing method capable of achieving higher structuring in nanocomposites with advanced multifunctional properties.

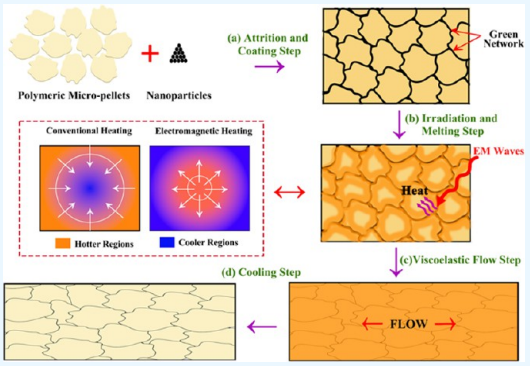

1. INTRODUCTION

For the last three decades, thermoplastic polymer nanocomposites (TPNCs) have been investigated as multifunctional materials[1−3] due to their potential for enhanced mechanical and transport properties and the advantages of the unique characteristics of polymeric thermoplastics.[4] Despite the advanced properties and exceptional characteristics of many commercially available nanoparticles (NPs), TPNCs prepared with such NPs often fall short of achieving exceptional strength, stiffness, and thermal and electrical conductivity.[5−7] Most times, this is attributed to hurdles like the lack of attaining structuring (i.e., orientation, conformation, crystallinity, segregation, crystal phases, interconnectivity, dispersion, distribution, etc.) in the TPNCs. Achieving controlled structuring is limited by intrinsic material (e.g., viscosity, crystallinity, molecular shape, particle's surface properties, particle's morphology, agglomeration, etc.) and processing parameters (e.g., mixing geometry, mixing time and speed, deformation rates, heat transfer, temperature, cooling rates, annealing, etc.) inherent to conventional processing methods.[8,9] This is fundamental because, for instance, without reaching NP dispersion, the remaining NP clusters behave like traditional microreinforcements, which limits the NP-matrix load transfer and the TPNCs' mechanical properties.[10,11] Concurrently, in the case of conductive NPs, clustering may contribute to NP interconnection via percolation, which yields thermal and electrical conductivity in the TPNCs.[12,13] In contrast, if excellent levels of NP dispersion are achieved, the transport properties are typically diminished due to the lack of NP interconnectivity.[14] Thus, achieving structuring in the produced materials is extremely important to attain targeted

Received: August 10, 2024
Revised: November 8, 2024
Accepted: November 15, 2024
Published: November 25, 2024

performance. Unfortunately, conventional processing methods like extrusion melt-mixing, *in situ* polymerization, and even solution casting are limited and inadequate for inducing advanced structuring.[5,15,16] To overcome this trade-off situation and achieve a balance between mechanical robustness and transport efficiency, innovative processing techniques are needed, capable of configuring or structuring the NPs in a way that they are both evenly segregated and distributed yet interconnected at different length scales in a defined network. Therefore, the pursuit of the next-generation TPNCs with precisely tuned nano- and microscale (i.e., multiscale) attributes calls for developing new and suitable processing methodologies that provide control over and tailoring of critical structural features in the TPNCs.

Since the introduction of microwave (MW) technology in the 1970s, MW heating or electromagnetic (EM) processing has revolutionized various industries due to its numerous benefits, including reduced power consumption (i.e., up to 70% less energy requirement), faster processing times, and eco-friendly operations.[14,17,18] The fundamental electromagnetic properties of materials such as electrical permittivity, electrical conductivity, and magnetic permeability (i.e., intrinsic impedance) play a crucial role in their EM susceptibility and EM absorption, which enable microwave processing.[19] Microwave irradiation can induce heating in nonmagnetic materials through two primary mechanisms: dielectric loss (or polarization loss) and conductive loss (or Joule heating). Dielectric loss occurs in materials with bound charges that either possess dipoles or that can be induced to form dipoles by an external electric field. Such dipoles can have an ionic, interfacial, or molecular (orientational) nature.[20,21] As the dipoles are polarized, energy is stored in the form of electric dipole moments. However, since the dipoles cannot respond instantaneously to the frequency of the applied field, their polarization starts to fall behind the field (i.e., become out of phase), causing dielectric damping and energy dissipation.[20,21] In contrast, conductive loss takes place in materials holding free charges (i.e., electrons or holes). The charges start to flow in the direction of the applied electric field, forming currents with magnitudes dependent on the conductivity of the material itself. As the flowing currents are formed, a counter-magnetic field is generated inside the material, which forces the charges in the reverse direction, thereby causing a frictional pathway for them, as well as energy dissipation. The oscillating EM field repeats this phenomenon rapidly, producing volumetric heating in the material.[22,23] Thus, owing to such complex conductive and dielectric loss phenomena, carbon nanotubes (CNTs), with their extended π-systems, undergo intense heating when exposed to microwaves, reaching temperatures as high as ∼2000 °C.[24,25] Moreover, gas plasma generation from absorbed gases like hydrogen in CNTs under microwave radiation can also contribute to localized superheating.[25] Polymers, in contrast, are virtually transparent to electromagnetic radiation in the microwave range and are not significantly heated by EM irradiation.[22,26]

In composite material systems, however, besides the intrinsic EM susceptibility of the particles themselves, their microscopic arrangement (i.e., their network type and configuration) and the macroscopic electrical dimensions of such particles' arrangement or network (i.e., physical length divided by the EM wavelength) play a deciding role in MW heating. First, having a network of conductive particles of comparable electrical dimensions to that of the wavelength of the EM field is necessary for an efficient EM coupling.[22] If the particles in the composite system lack enough interconnection, they form a capacitive network, and since the electrical permittivity of polymers is low, the restricted dielectric loss will lead to minimal heating, if any. On the other hand, if the particles are well-interconnected (i.e., percolated), their network is inductive, enabling significant Joule heating.[25]

Over the past five decades, the application of microwave heating in polymer processing has demonstrated significant potential, evolving from the curing of thermosetting elastomers and epoxy-based composites to welding, annealing, and joining thermoplastic-based materials.[27−30] Research efforts have mainly focused on the rapid and energy-efficient microwave curing of composite materials. Yingguang et al. demonstrated the energy-saving and fast-processing benefits of an indirect microwave heating method for curing multidirectional carbon fiber reinforced polymer composites, achieving significantly reduced curing cycle and energy consumption while improving mechanical properties compared to traditional thermal curing methods.[31] Chaowasakoo and Sombatsompop demonstrated that microwave-cured fly ash/epoxy composites required shorter curing times and exhibited higher impact strengths compared to those cured using conventional curing methods.[18] Thostenson and Chou demonstrated that microwave processing of polymer composites enables more efficient heat transfer compared to traditional methods, leading to rapid and uniform volumetric heating throughout the material thickness.[32] Furthermore, Zhou and Hawley found that using microwave energy for adhesive bonding significantly reduced the bonding time of polymer resins by accelerating the curing process compared to traditional thermal methods.[33]

Lately, microwave energy has been utilized for the sintering and welding of thermoplastics using CNTs. Sweeney et al.[28] demonstrated that CNT-based conductive inks can be used to weld three-dimensional (3D)-printed parts produced via fused deposition modeling, significantly increasing their interlayer bonding strength. The microwaved 3D-printed parts made with CNT-coated filaments improved their weld fracture strength by 275%, enhancing the mechanical properties of the thermoplastic 3D-printed components. Also, Wu et al.[26] investigated CNT-coated polypropylene particles for microwave welding of polypropylene macroscopic substrates. This study demonstrated the potential of CNTs to absorb microwave energy, generate heat, and effectively weld macroscopic thermoplastic parts. Likewise, Wang et al.[34] reported that a layer of carbon nanotubes applied onto a plastic substrate can easily melt its surface becoming part of the polymer substrate. They also reported that this method can also be used to strongly weld plastic parts in contact with a layer of CNTs in between them upon microwave irradiation, coining the term "microwave welding" and highlighting the possibility that this method may be a route to nanocomposite fabrication. Thus, up until now, for thermoplastics, the use of electromagnetic energy and CNTs has been limited to improving interlayer bonding in additive manufactured parts, welding macroscopic polymeric parts, and, lately, assisting with the sintering of polymeric beads for the casting of sintered nanocomposites.[27,35,36] Nevertheless, the use of EM energy to achieve electromagnetically induced viscoelastic melt-processing capable of fully melting thermoplastic domains to synthesize TPNCs from their separate constituents (i.e., nanoparticles and polymer pellets) has not been demonstrated. Because of this, we propose a unique processing method that

https://doi.org/10.1021/acsomega.4c07372
ACS Omega 2024, 9, 48546−48562

harnesses the heat generated from an electromagnetically susceptible green network of nanoparticles upon microwave irradiation, producing melting and viscoelastic flow of the host polymer matrix, leading to the fabrication of "monolithic" functional nanocomposites.[37] This method enables multiscale (i.e., from nano to macro) structuring of the TPNCs, leading to controlled segregated microstructural 3D networks that yield an innovative combination of properties in the TPNCs at very low NP loadings. Therefore, as the objective of this study, we carry out a systematic comparison between segregated CNT/polypropylene TPNCs prepared via conventional thermal melt-processing and segregated TPNCs synthesized and structured via our proposed EM melt-processing method. The microstructural, transport, and mechanical properties as well as the crystalline properties of the TPNCs are compared. We highlight the urgent need for scalable, efficient, environmentally friendlier, and rapid cutting-edge processing methods that use electromagnetic (EM) energy to enable controlled structuring in functional TPNCs. An understanding of such multiscale structuring that leads to a morphology with a segregated network formed by a defined interphase of CNTs, and of potential matrix−NP interfacial interactions induced by the EM energy in the TPNCs is necessary to elucidate fundamental microstructure−processing−properties relationships to enable the next generation of multifunctional TPNCs.

2. EXPERIMENTAL SECTION

2.1. Materials. Rotational molding grade polypropylene micropellets were procured from Matrix Polymers (U.K.), Revolve PP46 grade (designated as PP here). Such a PP grade has the following specifications: density of 0.905 g/cm^3, differential scanning calorimetry (DSC) melting point of 172 °C, Vicat softening point of 145 °C, and Melt Flow Index of 15.00 g/10 min. The particle size for PP was measured at 180 ± 29 μm via electron microscopy. Industrial-grade NC7000 multiwalled carbon nanotubes (CNT) with a nominal diameter of 8 nm, length of 10−30 μm, and BET surface area of 240 m^2/g were purchased from Nanocyl (Belgium).

2.2. Processing. The processing of the materials consisted of a dry mixing step using ball milling attrition that mingled and coated the polymer micropellets with CNTs, followed by mechanical compaction of the green mixtures to form "green" bodies that were subsequently melt-processed into TPNCs. Thus, CNT/PP nanocomposites were prepared for a range of selected concentrations: 0.3, 0.5, 1.0, 1.5, and 3.0 wt %. For comparison purposes, sets of the TPNCs were prepared via the proposed electromagnetic (EM) melt-processing as well as conventional thermal melt-processing using a hot press.

2.2.1. Formulation of Green Powders by Ball Milling Attrition. Initially, the PP micropellets were coated with CNTs via high-energy mechanical attrition using a Vertical High-Energy Planetary Ball Mill (Model: MSE PRO 4L by MSE Supplies) at such specified concentrations.[38] The ball milling process was conducted using dry conditions at 200 rpm utilizing a set of twenty -5 mm, ten 10 mm, and two 20 mm Stainless steel balls in each 500-mL Stainless steel jar. Batches of 50 g of formulated "powder" were prepared per jar for each concentration. The attrition process was kept at constant conditions for 60 min to ensure thorough mixing, mechanical exfoliation of the CNT primary agglomerates, and an even distribution of the nanomaterial on the surface of the PP micropellets. This processing step permitted achieving an exfoliated, predispersed, homogeneous, and interconnected layer of CNTs coating the top surface of the polymeric micropellets.

2.2.2. Green Body Fabrication. Following the formulation process, the coated micropellets were mechanically compressed at 18 tons and room temperature for 3 min using a hydraulic laboratory press (Carver Model 4389 MHC) and a 40 mm diameter Pellet Pressing Die Set (MSE Supplies) to form consolidated green bodies of about 1 g. This processing step enabled the structuring of the materials from the nano to the macro-scale in the form of a segregated arrangement with the exfoliated nanoparticles now forming a macroscopic interconnected network that scales the whole green body with electrical dimensions capable of interacting with the EM field of the microwaves. For each concentration, a set of ten green bodies (specimens) were produced from each ball-milled batch to ensure statistical validity (i.e., 5 replicates per processing method). Figure 1 displays on the left-hand side a photograph of a compacted green body.

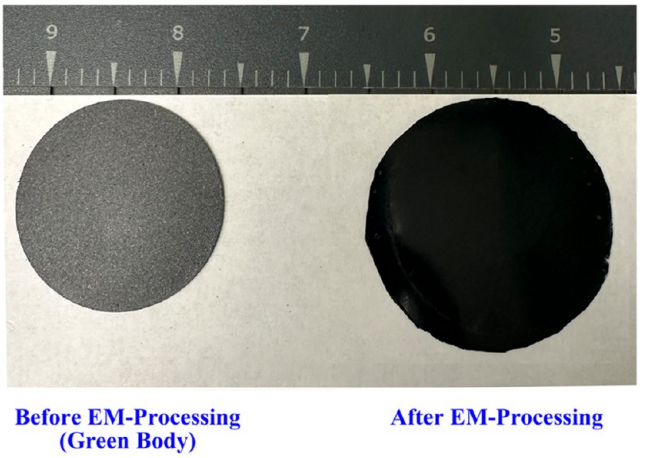

Figure 1. Photograph of the bodies before (left panel) and after (right panel) EM melt processing. The synthesized TPNC body (right panel) is larger as the material has experienced viscoelastic deformation and has become darker as the CNTs get fully integrated into the polymer matrix. Scale in inches.

2.2.3. Synthesis of the Nanocomposites. The formulated CNT/PP mixtures configured into green bodies were now melt-processed into nanocomposites via two alternative ways: conventional thermal heating using hot pressing vs microwave heating using the proposed electromagnetic melt-processing. Thus, 5 specimens were hot-pressed at 200 °C using a slight pressure (i.e., the weight of the press ∼35 lb) for about 6 min. Loctite 700-NC Frekote mold release was used to treat the metal surface of the molding plates prior to hot pressing to avoid the melt from sticking on the surface of the metal. The thickness (∼400 μm) of the formed TPNC specimens was controlled with metal spacers. Finally, cooling was applied to form the TPNC sheets. Likewise, hot pressing was used to process the neat PP into sheets using the same conditions. Subsequently, the other 5 green bodies were processed in a Microwave Research & Applications BP-095 UMISS Custom-made Laboratory Microwave Oven. Figure 2 displays a representative diagram of the laboratory microwave setup for the EM processing of the TPNCs. The green bodies were located in between two quartz flat slides and irradiated for less than 180 s with microwaves (2.45 GHz) at a constant delivered power of 500 W. The temperature of the specimens

https://doi.org/10.1021/acsomega.4c07372
ACS Omega 2024, 9, 48546−48562

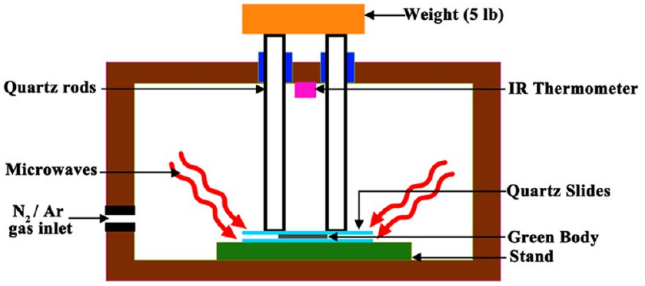

Figure 2. Schematic of the custom-made microwave oven setup in which the green bodies were EM melt processed between two quartz slides while applying a slight pressure with a 5 lb weight.

was monitored by using an infrared pyrometer (−50−975 °C range), but the reading took place at the surface of the quartz slide, which did not yield the exact sample's temperature (due to the low emissivity of quartz). Nevertheless, the temperature rise was a clear indication of the EM processing taking place. The custom-made oven has a True-to-Power magnetron capable of different settings levels and of delivering constant and specific power uniformly distributed within the oven chamber. When melting was reached and viscoelastic melt flow was attained, a slight mechanical force (∼5 lb) was placed manually on the top slide to slightly flatten the formed nanocomposite specimen to about 400 μm in thickness (a representative TPNC body is shown on the right-hand side of Figure 1). After irradiation, the TPNCs were allowed to cool down in between the quartz slides for a couple of minutes. A video of the viscoelastic melt flow induced by microwave irradiation on a green body as it turns into a TPNC is shown in the Supporting Section.

2.2.4. Electromagnetic Processing Conceptualization. The changes experienced by the material specimens during EM melt-processing are pictorially represented in Figure 3. In fact, Figure 3 outlines the sequential steps taken from the initial mixing stage of the constituents to the final structure developed upon irradiation and cooling. Initially, in the attrition and mixing step (a), the CNTs are exfoliated from the primary agglomerates, predispersed, and spread onto the surface of the PP micropellets, which are uniformly coated with CNTs. This step yields the "green mixture" formulations, which form a three-dimensional (3D) green network of nanoparticles upon the mechanical consolidation of the "green bodies" (i.e., unprocessed bodies). Such a network, formed by an interphase made of nanoparticles between the pellets, is now of macroscopic dimensions and has suitable electrical and dielectric properties that bring about an electrical length comparable to the wavelength of microwave radiation, yielding electromagnetic susceptibility to the green body.[39] In the irradiation and melting step (b), such susceptibility enables heat generation and heat transfer from the CNTs network into the bulk of the polymeric pellets, which causes melting, viscoelastic flow, polymer melt infiltration of the CNTs (engulfing), and a partial distortion of the network that depended on the viscoelasticity of the composite system and the level of deformation applied, step (c). Finally, in the cooling step (d), the material is allowed to cool down, solidifying into its final "frozen" microstructure. Crystallization and viscoelastic effects (e.g., trans-crystallinity, nucleating effects, induced crystal phases, nano viscoelastic relaxation, etc.), in the case of semicrystalline polymers, may also be produced by the presence of the interphase of CNTs now

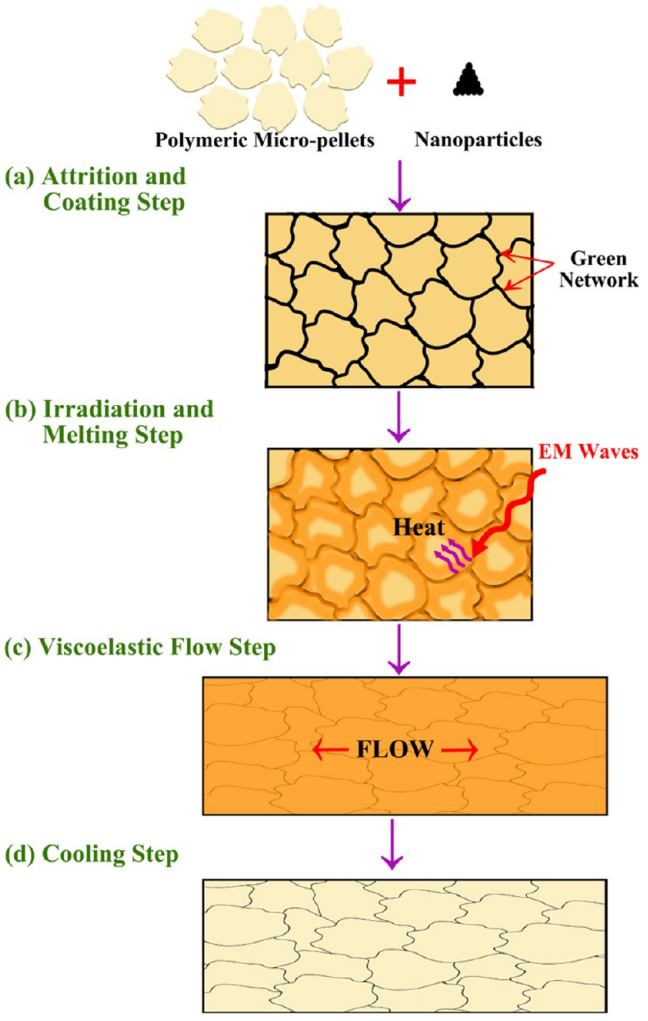

Figure 3. Conceptual representation of the steps involved in the proposed EM melt processing for the synthesis of segregated and structured TPNCs.

forming a partially deformed network that is responsible for a unique combination of mechanical, electrical, dielectric, thermal and even electromagnetic properties in the final TPNCs. This way, the sequential processing steps of attrition, compaction, irradiation, and cooling enable controlled structuring of the material into well-segregated TPNCs. We also hypothesize the possibility of other structural, chemical, interfacial, and crystallization effects induced by the EM inductive process itself on the TPNCs that may cause radical formation, matrix−NP chemical bonding, and even the formation of unusual crystal phases.

2.3. Testing and Characterization. *2.3.1. Mechanical Tensile Testing.* Tensile testing was carried out for all prepared nanocomposite concentrations and both processing methods. TPNC dogbone specimens were cut out from the processed specimens using a standard die cutter for tensile testing. For this, ISO 37 standard guidelines were followed as it includes one of the smallest dogbone standard geometries. Thus, dogbone specimens of about 400 μm in thickness were prepared with an ISO 37 Type 4 certified cutting die (Qualitest). An Instron Frame 5982 with the Bluehill Universal software with a 10 mm/min crosshead speed and a video extensometer (Instron Model: 2663−902), to record precise video strain (5 μm resolution), were used. An Instron 2580

https://doi.org/10.1021/acsomega.4c07372
ACS Omega 2024, 9, 48546−48562

load cell (5 kN) was used to record the load. Between 8 and 12 specimens were tested for each TPNC grade at room temperature ∼25 °C and ∼50% relative humidity. Four mechanical properties (i.e., Young's modulus, yield strength, tensile strength, and elongation-at-break) were obtained from the stress−strain curves.

2.3.2. Microscopy. The microstructure and morphology of the polymer micropellets, the green mixtures and bodies, and the nanocomposites were assessed by Scanning Electron Microscopy (SEM) using a JEOL JSM-7200 FLV FE microscope at 3 kV using secondary electrons mode. Before the inspection, the materials and cryo-fractured samples (to inspect the cross-section) of the TPNCs were subjected to a vacuum drying process to remove moisture and were coated with Gold/Palladium (Au/Pd 60:40) alloy for 60 s using a Denton Desk V TSC sputter coater. Image analysis of the SEM micrographs to quantify the diameter of the polymer micropellets was subsequently performed using ImageJ software (version 1.54d).

The NC7000 CNTs were also examined via SEM, but an acceleration voltage of 15 kV was used. Moreover, transmission electron microscopy (TEM) was used for the CNTs inspection, which was conducted on the same JEOL JSM-7200 FLV FE-SEM microscope with a Deben retractable motorized annular STEM detector operating at an acceleration voltage of 30 kV. For TEM, the CNTs were first dispersed in ethylic alcohol by ultrasonication for 30 s, and then a droplet of the suspension was applied onto a 3 mm copper grid for observation.

2.3.3. X-ray Diffraction (XRD). X-ray diffraction (XRD) analysis was performed to characterize the crystalline properties of the CNTs and their nanocomposites, including both EM-processed and hot-pressed specimens. The XRD analysis was carried out using a Bruker D8 Advance X-ray Diffractometer equipped with Cu $K\alpha_2$ radiation. The diffractometer was operated at an energy setting of 40 kV and a current of 40 mA. Scans were conducted over a 2θ range from 10 to 60° for the CNTs and from 5 to 35° for the TPNCs. The angular step size was set at 0.05° to achieve high-resolution data, with a scan rate of 5.0° per minute.

2.3.4. Electrical Conductivity. Electrical conductivity measurements were conducted using a Keithley 6517B High-Resistance Electrometer connected to a customized in-house-made resistivity test fixture that may accommodate specimens of different sizes. This setup adhered to the ASTM D257 standard for high-resistance measurements. The alternating polarity method was employed for data acquisition, utilizing the Keithley KickStart Software. Suitable voltages ranging from 1 to 500 V were applied during measurements to prevent thermal noise during the measurements and to cover a readable current range (pA to mA), with multiple replications per specimen performed to ensure accuracy and precision. Through-thickness resistance measurements of the materials (i.e., green bodies and TPNCs) were obtained. The relative humidity (RH) of the experimental environment, approximately 50% RH at the time of measurements, was monitored using a commercial humidity probe. The volume electrical conductivity, σ, was then calculated using eq 1 from the resistance, R, measurements and the specimen's dimensions (i.e., thickness, l, and cross-sectional area, A).

$$\sigma = \frac{l}{RA} \tag{1}$$

2.3.5. Differential Scanning Calorimetry (DSC). Differential scanning calorimetry (DSC) analyses were performed utilizing a TA Instruments Q100 DSC analyzer, operating under a nitrogen atmosphere with a flow rate of 50 mL min^{-1}. Duplicate samples with a mass range between 5 to 10 mg were selected from the pristine polypropylene, the EM-processed TPNCs, and the hot-pressed TPNCs. The analysis protocol comprised five thermal cycles to obtain the thermal transitions of the materials. Initially, the samples were heated from room temperature to 200 °C at a heating rate of 10 °C min^{-1}. This first heating cycle aimed to remove any residual thermal history. Subsequently, an isothermal hold at 200 °C for 5 min was applied to stabilize the temperature. Following this, the samples were cooled at 10 °C/min to 25 °C to promote controlled crystallization. Afterward, a second isothermal condition at 25 °C for 5 min was implemented to preserve the newly formed crystalline morphology. A final heating cycle at 10 °C min^{-1} from 25 °C back to 200 °C was then conducted to examine the history-free melting behavior of the samples. The cold crystallization temperature (T_{cc}), and melting temperature (T_m) were determined from the second heating scan, while the crystallization temperature (T_c) was taken from the quenching step. The peak temperature associated with each thermal transition was determined through the linear extrapolation of the corresponding tangents. Experiments were executed by duplicates.

3. RESULTS AND DISCUSSION

3.1. Microstructure. Figure 4 displays a representative SEM micrograph of the PP polymer micropellets on a porous carbon conductive adhesive tape. The pellet size was obtained with an average of 180 μm with a standard viability of 29 μm. The micropellets displayed an irregular shape with a rough surface which allows CNTs to stick to their surface. The morphology of the NC7000 CNTs is shown in Figure 5 at different magnifications. The CNTs are forming large primary agglomerates as large as 300 μm in diameter (Figure 5a), the agglomerates, in turn, are formed by entangled CNT bundles (Figure 5b), the bundles are made of very long CNTs (as large as tens of microns, Figure 5c) and of diameters between 5 and 20 nm (Figure 5d).

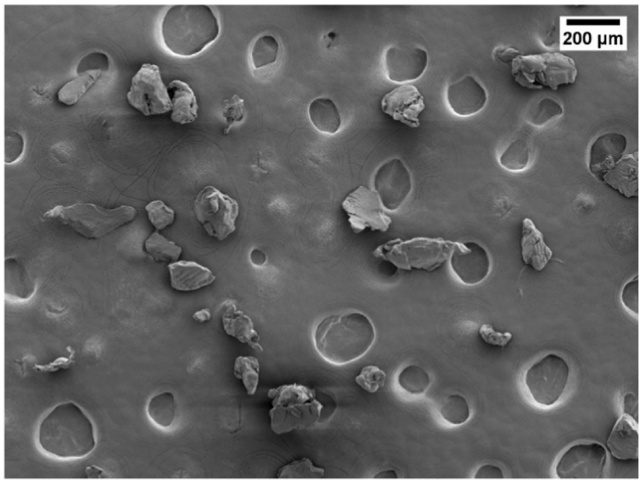

Figure 4. Electron micrograph of the polypropylene (Matrix Polymers Revolve PP46) micropellets used in this study displayed on the surface of a conductive carbon tape.

https://doi.org/10.1021/acsomega.4c07372
ACS Omega 2024, 9, 48546−48562

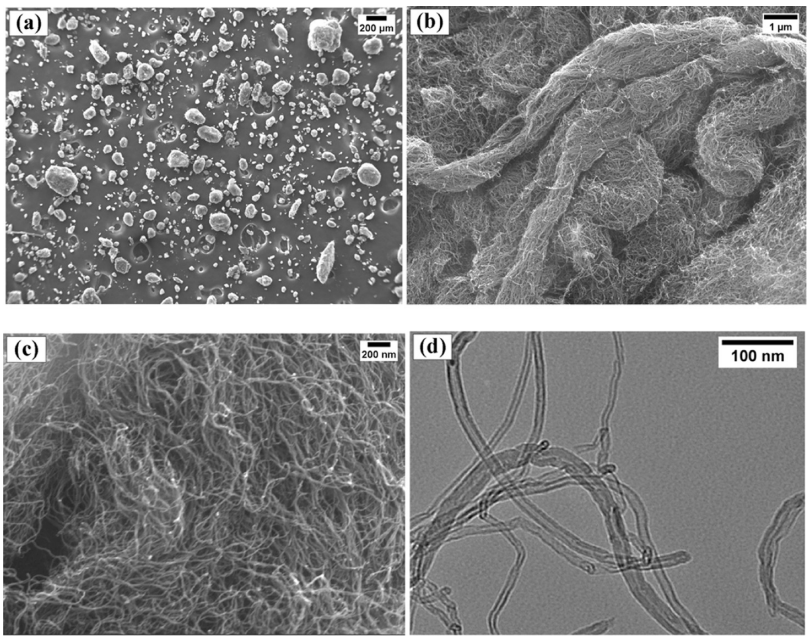

Figure 5. Electron micrographs of NC7000 carbon nanotubes at different magnifications showing from primary agglomerates, bundles, to wall morphologies: (a) ×30, (b) ×10,000, (c) ×35,000, and (d) ×400,000.

The microstructure and morphology of the green mixtures and bodies were also assessed. The SEM images displayed in Figure 6 reveal that, at a CNT concentration of 1 wt %, the green mixtures and bodies exhibited a satisfactory distribution and exfoliation of CNTs from their primary agglomerates, which is attributed to the different milling mechanisms (e.g., crushing, shearing, smashing) encountered during the ball milling process carried out with multiple balls of different sizes.[40] Thus, the polymer micropellets in the green mixtures showed a uniform thin layer of interconnected CNTs coating their surface (Figure 6a). The absence of significant agglomeration across various examined sites and magnifications is noteworthy, which gives an impression of reaching a pseudodispersed state caused by the uniform distribution of the CNTs all over the surface of the pellets in the green bodies (Figure 6b shows the cross-section of a green body). Once in the compacted green body (Figure 6c), the coated micropellets form a uniformly segregated multiscale network that encompasses from the nanoscale of the CNTs, passing through the microscale of the micropellets to the whole macroscopic length-scale of the green body. Such a network not only depends on the intrinsic properties of the NPs and the attrition conditions that control the exfoliation and interconnectivity of the NPs (as the aspect ratio of the CNTs may also be affected by the milling conditions) but also on the shape of the micropellets themselves and their relative superposition and fit imposed by the compaction conditions.

Once the green materials were processed, the resulting TPNCs were also inspected by electron microscopy for a qualitative assessment of their resulting morphology, dispersion, and distribution. Figure 7 displays representative SEM micrographs of the cross-section of the EM-processed TPNCs at 1 wt %. Like in the case of the green bodies, the EM-processed TPNCs also exhibited, at low magnifications, an apparently good dispersion with most CNTs fully engulfed by the melted polymeric matrix at macroscopic levels (Figure 7a,b). Such apparent dispersion also comes from the even and fine distribution of the CNTs on the surface of the "coated" micropellets and from the high exfoliation of the CNT primary agglomerates attained by the dry mixing step. This apparent dispersion is quite evident in the SEMs, as no significant agglomeration was found across various examined locations and magnifications. Nevertheless, as shown in Figure 7c, a well-defined thin layer of segregated CNTs can evidently be observed at higher magnifications at several locations across the cross-section. A few small (~3 μm) CNT clusters were occasionally identified as well (Figure 7c), also forming part of such layer of CNTs. In fact, Figure 7c,d, and e show the reminiscences of a discernible thin and long interphase of CNTs, circumscribed in red, which is the "boundary" that 4 or 5 adjacent micropellets shared in the original green body, and that now has been deformed by the induced melt flow. The CNTs at the interphase were exfoliated from the original primary agglomerates and are now distributed all over the surface area of the melted micropellets. To some extent, they are also dispersed (i.e., not agglomerated) within the interphase, but they continue interconnected, forming a three-dimensional percolated network. This level of tailoring and control of the structure (i.e., structuring) enables the difficult achievement of a simultaneously well-segregated and "dispersedly" interconnected multiscale network within the TPNCs. In other words, this method facilitates the elimination, or at least the size reduction,[41] of CNT agglomerates (i.e., exfoliated) without losing much of the interconnection of the segregated network. Thus, the EM inductive volumetric heating processing, that takes place at and from the very CNTs interphase of these preconfigured nano- and micro-materials, enables control of the interfacial and interphase features and bulk microstructure of these composite systems. Indeed, if the heating process takes place long enough, the material will experience full bulk melting and viscoelastic flow that can lead to excessive deformation. This distorts the initially configured NP network in the green body, affecting all the properties of the material. Therefore, not only parameters like micropellet size, size distribution, shape, matrix viscosity, NPs intrinsic susceptibility, aspect ratio, and attrition

https://doi.org/10.1021/acsomega.4c07372
ACS Omega 2024, 9, 48546−48562

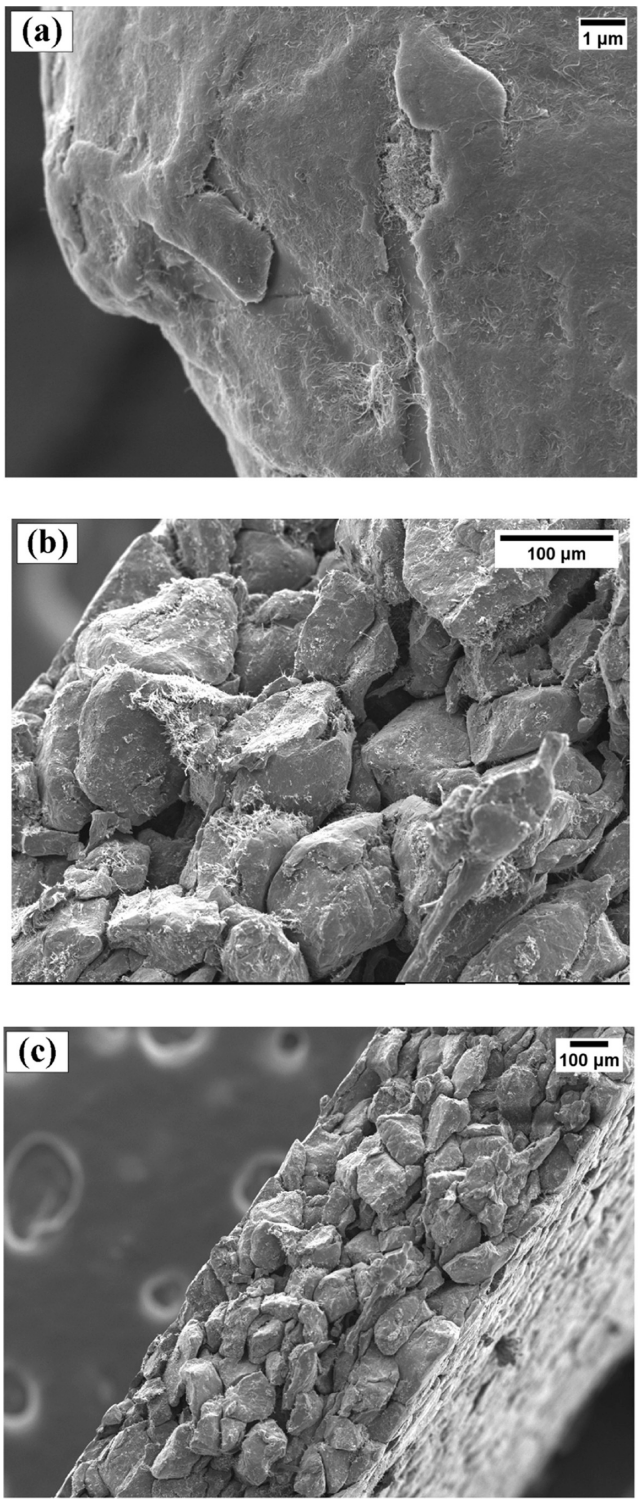

Figure 6. Electron micrographs of the formulated "green bodies": (a) a single micropellet coated with NC7000 CNTs, (b, c) cross-sectional views of a compressed green body at different magnifications.

conditions play a role, but also factors like deformational stresses, fusion enthalpy, heat capacity, viscoelasticity, irradiation time and power are important to configure the final network and properties of the resulting TPNCs.

Another important observation worthy of discussion is that for some particular EM-processing conditions, the formation of some voids or pores in the TPNCs was observed. Figure 7 displays some voids in a few locations of the cross-section of the TPNCs. This occurrence may primarily be attributed to the presence of microsized air pockets in the green bodies or to localized overheating at interpellet interstices where the local concentration of CNTs is too large. The second hypothesis seems more feasible as, sometimes, when the power is not well controlled during irradiation, some samples release some degassing. These effects were drastically reduced by utilizing a noncycling magnetron power controller (True-to-Power) and an inert atmosphere (N_2 gas) within the custom-made microwave chamber. However, defects are intrinsic under nonideal conditions and may have affected the mechanical properties of the specimens. More investigation on processing conditions may lead to defect-free specimens in the future.

In contrast to the EM-processed TPNCs, Figure 8 presents SEM images of the cross-section of the conventionally processed TPNCs at 1 wt %. The micrographs of the hot-pressed TPNCs confirm that, like the EM-processed materials, conventional processing also tends to keep the CNTs segregated in a network. Little flow was induced into the material during hot pressing to prevent excessive distortion. Actually, shear rate levels similar to those experienced by the EM-processed specimens were targeted here for comparison purposes. However, conventional processing took much longer, of the order of 6 min, to attain enough consolidation of the TPNCs, which may have caused more momentum transfer and network distortion than in the case of the EM-processed TPNCs. In fact, Figure 8b–d show a considerable penetration of CNTs into the bulk matrix in the hot-pressed TPNCs when compared to that of the EM-processed TPNCs. Conventional heating led to a more diffused interphase as CNTs are spread over wider areas and not within well-defined boundaries (more like clusters), lacking defined interphase lines as in the case of their microwaved counterparts. This is likely because, for energy to reach the inner bulk of the material, full melting must have taken place first in the outer zones of the material, pushing for a type of shearing melt flow. This causes laminar momentum transfer from the outer regions toward the colder ones, causing a more pronounced divergence of the layers and the CNTs contained between them and, as a result, a large distortion of the initial green network.

These results indicate that the electromagnetic melt processing, with its volumetric heating localized at the interphase, facilitated the retention of a more defined 3D network of NPs, which will have profound implications on the properties of the thus synthesized TPNCs. Given the conductive nature of CNTs, such a continuous and conductive 3D network could impart the material with extremely low electrical percolation threshold levels and enhanced electromagnetic interference (EMI) shielding effectiveness, which are highly desirable in various electronic and photonics applications. Furthermore, the 3D network obtained may also lead to a simultaneous improvement in mechanical properties, as it may behave as a semicontinuous multiscale reinforcement that spans from the nano to the full macroscopic dimensions of the TPNC. Moreover, SEM analysis demonstrated that the synergistic application of dry attrition of particles of different scales facilitated the segregation, distribution, and homogeneity of the material as exfoliation and primary agglomerate size reduction took place effectively during the ball milling process, giving a sense of reaching a "dispersed" but interconnected configuration of nanoparticles around the microscale of the pellets.

https://doi.org/10.1021/acsomega.4c07372
ACS Omega 2024, 9, 48546−48562

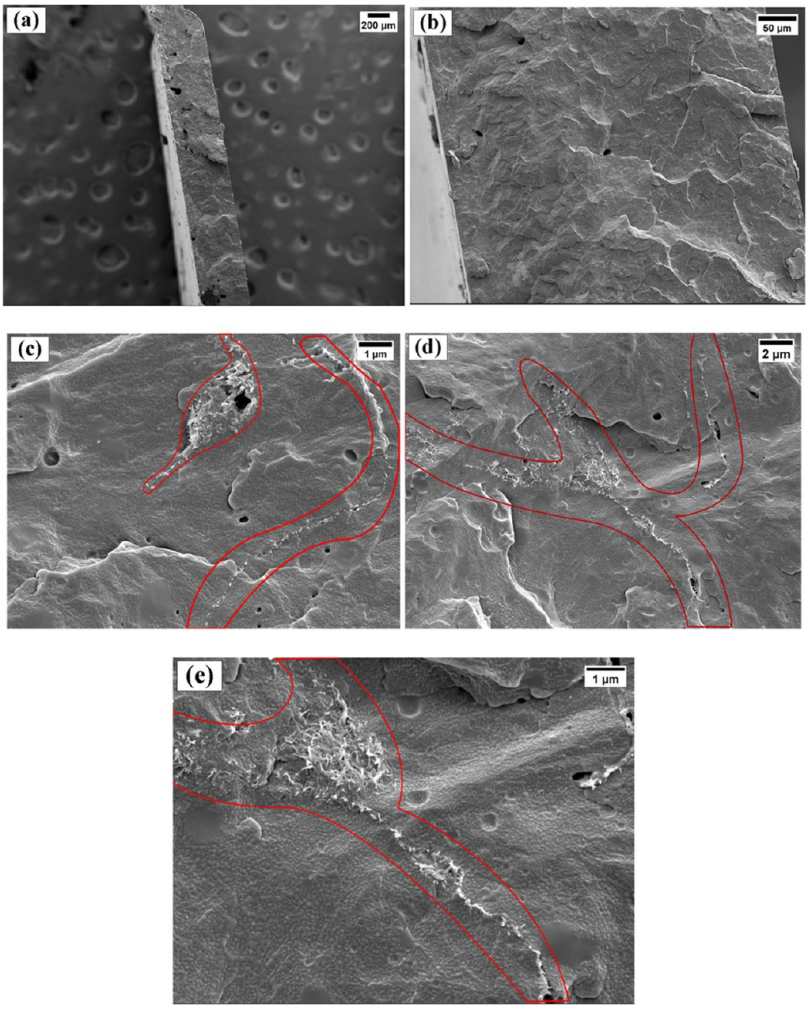

Figure 7. Representative scanning electron micrographs of the cross-section of the EM-processed TPNCs (a) low magnification, (b) medium magnification, (c–e) high magnification at two different locations showing the interphase of exfoliated CNTs forming a segregated but interconnected network.

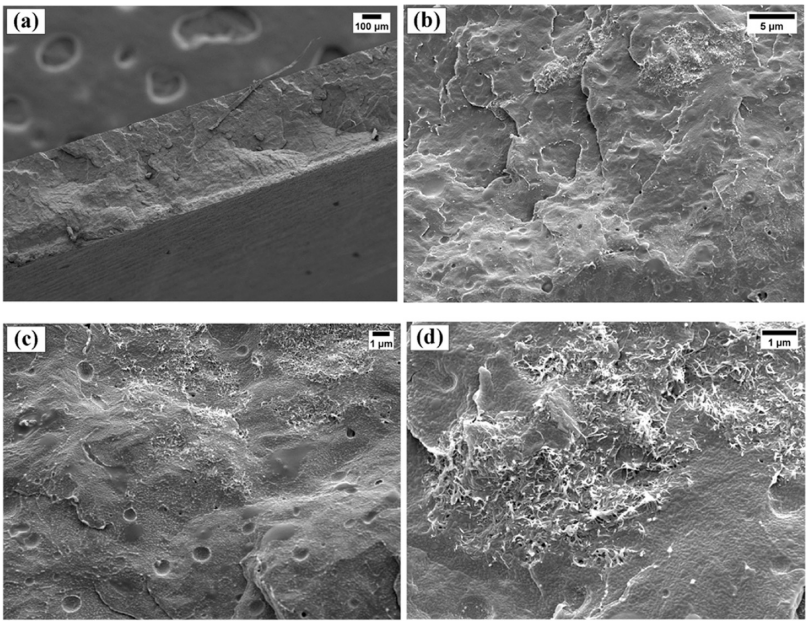

Figure 8. Representative scanning electron micrographs of the hot-pressed TPNC samples at different magnifications, (a) macroscopic cross-section, (b, c) diffused CNT interphases in the TPNCs and (d) high magnification of the diffused CNT interphase.

https://doi.org/10.1021/acsomega.4c07372
ACS Omega 2024, 9, 48546–48562

3.2. Percolation and Electrical Conductivity. Figure 9 shows the volume electrical conductivity (VEC or σ) of the

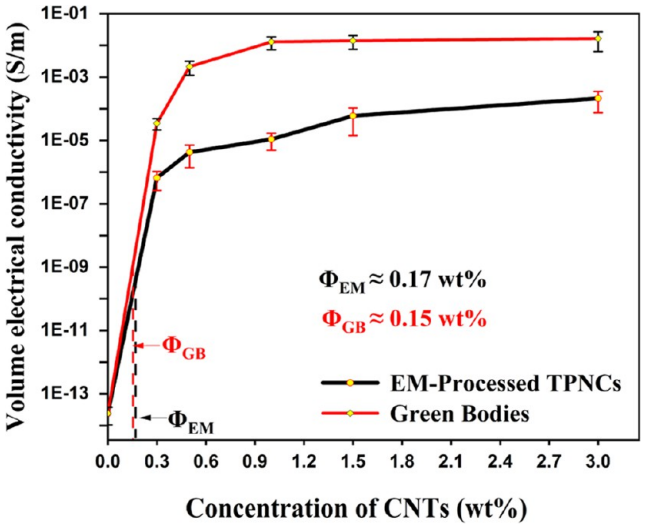

Figure 9. Volume electrical conductivity of green bodies and their respective EM-processed TPNCs at the corresponding CNT concentrations.

green bodies and their respective EM-processed TPNCs as functions of concentration. In general, and consistently with percolation theory,[42] the VEC increases following a power law as the particle concentration increases for both systems. Interestingly, before and after EM irradiation processing, the materials exhibited percolation threshold, Φ, values of about 0.15 and 0.17 wt % (i.e., ∼0.09 vol %), respectively. Incorporating CNTs alone significantly enhanced the conductivity of the green bodies, increasing it by nearly 12 orders of magnitude, from $(2.406 \pm 1.353) \times 10^{-14}$ S/m of the insulating PP matrix to $(1.292 \pm 0.562) \times 10^{-2}$ S/m at only 1.0 wt %, reaching a limiting plateau. Likewise, the EM-processed TPNCs' conductivity increased by nearly 9 orders of magnitude, reaching $(1.095 \pm 0.6033) \times 10^{-5}$ S/m at 1.0 wt %. Such percolating behavior has to do with the high level of network formation within the whole scale of the materials that keep exfoliated and spread but interconnected CNTs (due to the high aspect ratio of the CNTs) on the surface of the micropellets in the green bodies and within well-defined interphases in the EM-processed TPNCs. This effective interconnection between NPs is instrumental in enhancing the conductive properties of the composite material.[43,44] The reduction of about 3 orders of magnitude in conductivity for the EM-processed TPNCs with respect to the green bodies at the same compositions is believed to come from the partial distortion that the induced melt flow produces on the network. Microscopical evidence for this was presented earlier in Figures 6 and 7.

As the CNT concentration increased beyond 1 wt %, both green bodies and TPNCs demonstrated a leveling-off conductivity (plateau), indicating that a percolated network was established early on and that further addition of CNTs does not significantly improve conductivity. This saturation effect is a hallmark of the percolation theory and suggests that a critical concentration exists (i.e., the threshold) beyond which the benefits of additional filler are marginal.[44] Interestingly, the percolation threshold appears to occur at nearly the same concentration for both systems, i.e., prior to and after irradiation, suggesting uniformity in the conductive network's initial development and indicating that microwave processing does not affect the size or aspect ratio of the CNTs, unlike other conventional processing techniques like extrusion.

Figure 10 displays a comparison of the volume electrical conductivity of EM-processed TPNCs vs that of the conventionally processed TPNCs. A summary of the average volume electrical conductivity data and their variability for the EM-processed and the hot-pressed TPNCs are also presented in Table 1. The behavior of both systems is shown as a function of CNT concentration up to 3.0 wt %. As expected, an increase in the CNT weight percentage increases the conductivity of the TPNCs obtained via both processing techniques. Nevertheless, the hot-pressed TPNCs exhibited a percolation threshold value between 1.5 and 3.0 wt % (i.e., about 2.0 wt %), which is significantly higher than their EM-processed TPNCs (i.e., about 1 order of magnitude higher). Additionally, for the hot-processed TPNCs, their conductivity at $(2.046 \pm 1.276) \times 10^{-13}$ S/m at 1.0 wt % was statistically the same as that of pure PP (i.e., $(2.406 \pm 1.353) \times 10^{-14}$ S/m). In contrast, the volume electrical conductivity value obtained at 1 wt % for EM-processed TPNCs is $(1.095 \pm 0.6033) \times 10^{-5}$ S/m, representing an increase of nearly 8 orders of magnitude compared to hot-pressed TPNCs. The higher percolation threshold observed in the hot-pressed TPNCs may be ascribed to the formation of the more "diffuse" network with less interconnectivity promoted by the laminar momentum transfer that spreads the CNTs into a more diffusive interphase region. This can be backed up with microstructural and morphological observations previously discussed in the microstructure section. This phenomenon is pictorially represented in Figure 11a. This reduced CNT interconnection imposed by a "diffused" interphase and by some discontinuities in the network itself is likely provoked by the higher deformation brought about by conventional heating. In other words, conventional processing does not yield efficient conductive pathways at lower CNT loadings, limiting the early formation of a fully percolated three-dimensional conductive network. In

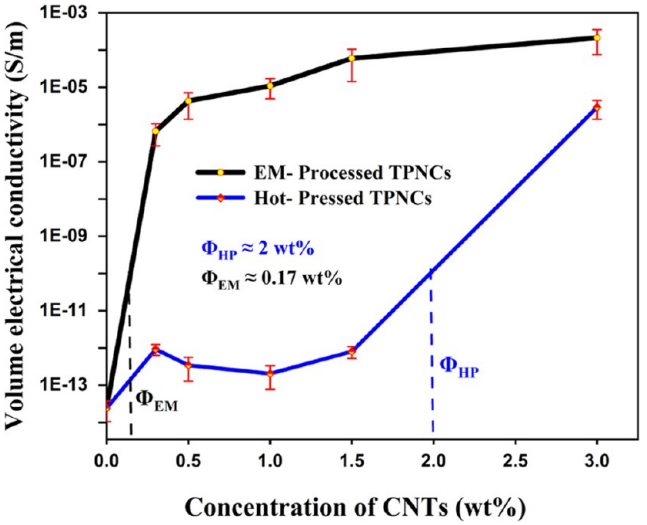

Figure 10. Comparison of the volume electrical conductivity of the EM-processed TPNCs vs that of the hot-pressed TPNCs as functions of concentration.

https://doi.org/10.1021/acsomega.4c07372
ACS Omega 2024, 9, 48546−48562

Table 1. Average Volume Electrical Conductivity of the EM-Processed TPNCs, Hot-Pressed TPNCs, and the PP Matrix[a]

formulation	green bodies (S/m)	EM-processed TPNCs (S/m)	hot-pressed TPNCs (S/m)
PP	$(2.406 \pm 1.353) \times 10^{14}$	$(2.406 \pm 1.353) \times 10^{-14}$	$(2.406 \pm 1.353) \times 10^{-14}$
0.3% CNT/PP	$(3.509 \pm 5.349) \times 10^{5}$	$(6.602 \pm 3.946) \times 10^{-7}$	$(9.311 \pm 3.031) \times 10^{-13}$
0.5% CNT/PP	$(0.002 \pm 0.002) \times 10^{\circ}$	$(4.274 \pm 2.886) \times 10^{-6}$	$(3.417 \pm 2.133) \times 10^{-13}$
1.0% CNT/PP	$(0.120 \pm 0.005) \times 10^{\circ}$	$(1.095 \pm 0.603) \times 10^{-5}$	$(2.046 \pm 1.276) \times 10^{-13}$
1.5% CNT/PP	$(0.0140 \pm 0.006) \times 10^{\circ}$	$(5.998 \pm 4.571) \times 10^{-5}$	$(8.063 \pm 2.838) \times 10^{-13}$
3% CNT/PP	$(0.016 \pm 0.0120) \times 10^{\circ}$	$(2.136 \pm 1.379) \times 10^{-4}$	$(2.911 \pm 1.516) \times 10^{-6}$

[a]Variability values are 95% confidence intervals.

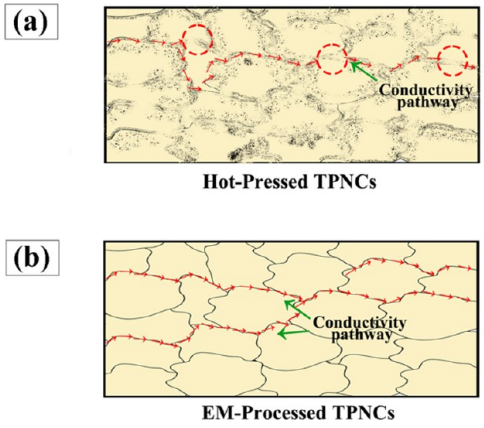

Figure 11. Pictorial representation of the electrically conductive pathways developed in the microstructure imposed by the processing method for (a) hot-pressed TPNCs and (b) EM-processed TPNCs.

contrast, Figure 11b depicts the situation for the EM-processed TPNCs in which a sharper and more CNT-interconnected interphase leads to a stronger network that enables more percolative electron transfer across the TPNC.

The percolation threshold is influenced by several factors, including particle size, aspect ratio, clustering level, shape, phase adhesion, interfacial interactions, and spatial configuration and conformation of the polymer molecules, which are highly determined by processing conditions.[44,45] Furthermore, the significantly faster processing associated with microwave irradiation may be responsible for increased penetration of the PP molecules into the remaining CNT clusters and bundles (i.e., localized melt infiltration) and even into the CNT structure itself without the need for significant melt flow, preserving this way the original "green" network structure within the PP polymeric matrix. Very importantly, the microwave irradiation inductive step may even be responsible for the generation of free radicals, which may, in turn, be playing a role in increasing interfacial interactions and reactions between the PP matrix molecules and the heated surface of the CNTs located in the vicinity of the interphase region. This hypothesized chemically linked electromechanical network may have meaningful effects on the elasticity and ultimate mechanical properties of the TPNCs and may be the key to unveiling the concurrent achievement of advanced transport and mechanical properties in the TPNCs.

3.3. Crystal Structure. Figure 12 presents the XRD diffractograms for the neat PP and its TPNCs processed via both methods for selected CNT concentrations. Both the neat PP and the TPNCs exhibit characteristic reflections of the crystalline α-form of PP at 2θ values of 14.15° (110), 17.00° (040), 18.61° (130), 21.16° (111), 21.90° (131), and 25.40° (060).[46,47] A notable peak at 2θ = 16.20°[48] signals the presence of the β-crystal form (300) within the PP polymer structure. However, such a peak decreases in intensity in the TPNCs, supporting the well-known fact that CNTs promote crystallization.[48] In Figure 12a, a comparison of the XRD diffractogram of the pristine PP matrix to those of the TPNCs at 0.5 wt % is displayed. The diffraction angles remain largely unchanged, with the notable disappearance of the peak at 16.20° in the EM-processed TPNCs, and a considerable reduction in peak intensity in the hot-pressed TPNCs. The reduction of such a peak suggests an alteration in the crystalline structure and points to a significant phase transformation,[49] from the β to the α phase. Nevertheless, as displayed in Figure 12b,c, at higher CNT contents, both processing methods primarily favored α phase formation. According to Zhang et al., it is well-established that α-crystalline phases are more thermodynamically stable. The remarkable reduction in peak intensity in the EM-processed TPNCs may be attributed to the rapid and localized heating characteristic of EM processing, which preferentially promotes the formation of the more thermally stable α phase at elevated temperatures quicker than conventional processing.[50]

Phase transformations from β to α in polypropylene nanocomposites as well as changes in their crystallinity content not only potentially alter their electrical properties but also impact their mechanical robustness. Studies consistently show that β-PP enhanced toughness over α-PP, a trait linked to molecular characteristics and crystallinity.[51] Such characteristics are essential for the mechanical enhancements seen with these transformations in nanocomposites.[52,53] Jeon et al. highlighted that the electrical conductivity of single-walled carbon nanotube (SWCNT)/PP nanocomposites decreases significantly with a reduction in crystallinity, especially when their SWCNT concentration falls below the percolation threshold.[54] Their findings showed that at 0.3 wt % SWCNT, reducing the crystallinity from 70 to 10% causes the conductivity to decrease by more than 4 orders of magnitude.[54] The electrical conductivity of a composite depends largely on the dispersion and the arrangement of the filler's network. The dispersion and arrangement of CNTs are, in turn, notably affected by the polymer's ability to crystallize. Therefore, the crystalline properties of the polymer matrix are crucial in determining the electrical and dielectric properties of the composites. Moreover, crystallinity may affect not only the conductivity but also the dipole polarization of the molecular groups and segments.[55] Thus, other changes in the PP crystallization characteristics, such as the increased intensity of the (040) crystal planes, as highlighted in Figure 12a (i.e., inserted subplot in the top right corner), are likely to influence the dielectric properties of the TPNCs as well.[55] Besides the differences in the attributes of the CNT networks developed in the TPNCs by both processing methods, the distinct crystallization characteristics observed in the EM-

https://doi.org/10.1021/acsomega.4c07372
ACS Omega 2024, 9, 48546−48562

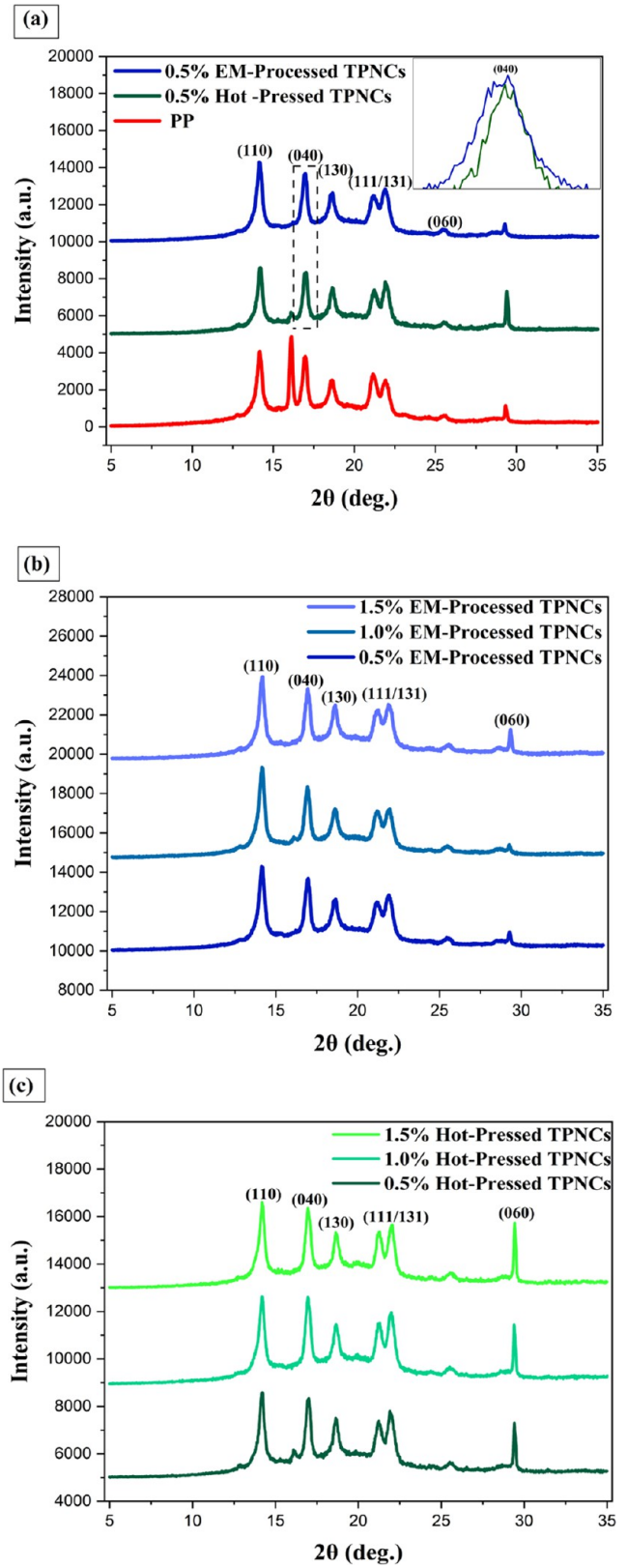

Figure 12. XRD diffractograms of (a) a comparison of 0.5 wt % TPNCs and the PP matrix, (b) EM-processed TPNCs, and (c) hot-pressed TPNCs at selected concentrations.

processed TPNCs may also be contributing, to some extent, to the notable enhancement in conductivity.

3.4. Crystallization Behavior of the TPNCs. Figure 13 displays plots of the DSC thermograms for the PP matrix, the

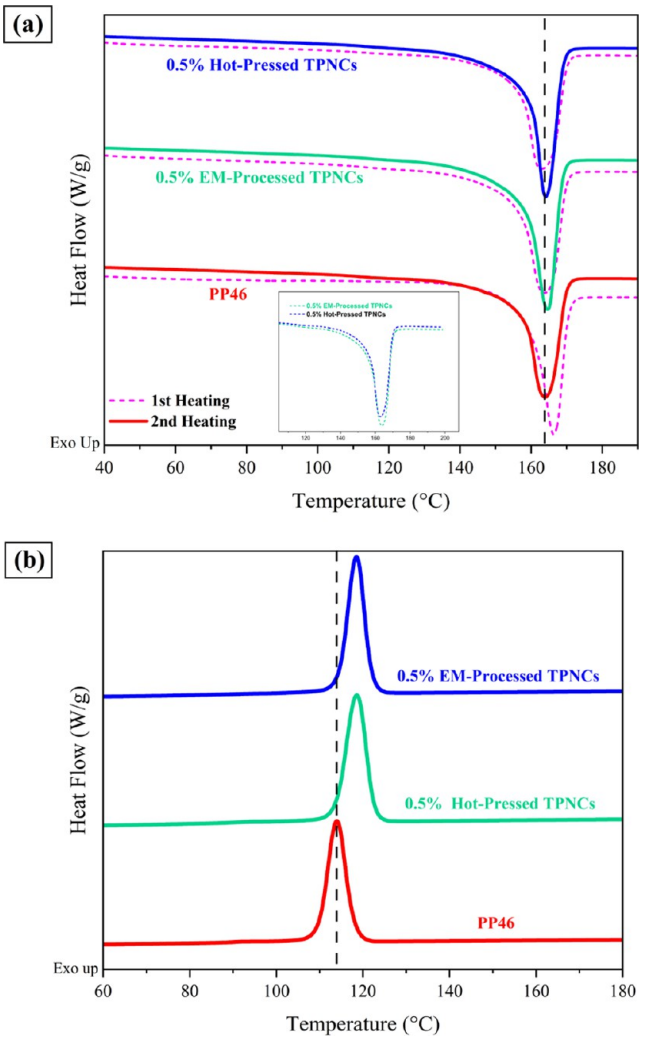

Figure 13. Comparative DSC thermograms for pristine PP and its TPNCs, (a) first and second heating cycles, and (b) cooling cycle.

0.5 wt % EM-processed TPNCs, and the 0.5 wt % hot-pressed TPNCs. The first and second heating cycles are shown in Figure 13a as broken and solid lines, respectively. The cooling cycle is presented in Figure 13b. The vertical discontinuous lines are drawn to mark the T_m (Figure 13a), and T_c (Figure 13b) values, corresponding to the thermal transitions, melting temperature, and crystallization temperature, respectively. Table 2 provides a summary of the thermal properties obtained from the DSC analysis of the materials, including the crystallization temperature (T_c), the crystallization enthalpy (ΔH_c), the melting temperature (T_m), the melting enthalpy (ΔH_m), and the percentage of crystallinity obtained from the first x_{c_1} and second x_{c_2} heating cycles.

According to the second heating cycle, the PP matrix shows a T_m of 163.90 °C, which is consistent with values reported in the literature (e.g., 163−164 °C).[56] When considering the second heating cycle, EM-processed and hot-pressed TPNCs displayed T_m values of 164.63 and 164.13 °C, respectively. This small difference of 0.5 °C in T_m may be indicative of a variation in the crystal structure, but this difference is too small to be conclusive about this.[57] The incorporation of CNTs into

https://doi.org/10.1021/acsomega.4c07372
ACS Omega 2024, 9, 48546−48562

Table 2. Thermal Transitions and Data Obtained from DSC Analysis of Different Materials

material	T_m (°C)	T_c (°C)	ΔH_c (J g^{-1})	ΔH_m (J g^{-1})	x_{c_1}(%)	x_{c_2}(%)
PP	163.90	113.88	78.02	45.70	30.93	32.44
0.5% EM-processed TPNCs	164.63	118.55	86.13	40.60	83.22	85.68
0.5% hot-pressed TPNCs	164.13	118.40	80.47	18.40	76.79	78.78

the PP matrix shifts T_m to slightly higher temperatures, suggesting an enhancement in lamellar thickness and a refinement in the crystallite structures.[46] When crystals are perfect, they exhibit a sharp, well-defined melting peak and higher melting enthalpy, meaning, there is a larger energy barrier to deform or break the crystals during melting. Research by Jeon et al. showed that in isotactic PP nanocomposites, the crystals are expected to be thicker than those in unfilled PP, which explains the modest 3−4 °C increase in melting temperature.[54] When comparing the T_m values from the first and second heating cycles, it can be seen that the second cycle shows a ∼2 °C decrease in temperature, which signals an effect of processing consistent with the XRD studies. The inserted plot in Figure 13a shows a slight difference in the first-heating melting enthalpy in the TPNCs obtained via the two processing methods, the enthalpy by EM processing was higher than that by thermal processing. As we discussed earlier, crystals obtained during the EM processing might be more perfect than those developed in the hot-pressed TPNCs, which is why EM-processed TPNCs showed higher melting enthalpy.

The percentage of crystallinity was calculated by the following eqs 2 and 3[58]

$$x_{c_1} = \frac{\Delta H_m - \Delta H_{cc}}{\Delta H_m^0} \times 100\% \quad (2)$$

$$x_{c_2} = \frac{\Delta H_m}{\Delta H_m^0} \times 100\% \quad (3)$$

where ΔH_{cc} is the enthalpy of cold crystallization, and ΔH_m^0 is the melting enthalpy of pure crystals (i.e., 207 J g^{-1} for pure PP[46]). In the first-heating cycle, ΔH_{cc}, is negligible in all three cases. Thus, it was ignored during the calculations.

As indicated in Table 2 and Figure 13b, relative to pristine PP, the EM-processed TPNCs displayed a 4.67° increase in T_c (118.55 °C), while the hot-pressed TPNCs exhibited a similar T_c of 118.40 °C. The addition of CNTs can influence the crystallization behavior of polypropylene in TPNCs in two main ways.[59] First, CNTs have a large surface area, which provides a greater amount of nucleation sites for PP molecular chains to attach to and to be arranged in an orderly manner.[60] Second, CNTs can hinder the mobility and diffusion of PP chains in the undercooled melt, which is essential for crystallization.[59] This reduced chain mobility increases stiffness at lower CNT loadings.[61] As the concentration of CNTs continues to rise, a more interconnected CNT network forms, further restricting the diffusion of PP chains and thereby influencing the crystallization process.[62] Consequently, employing CNTs as nucleating agents can effectively promote the crystallization of PP at elevated temperatures.[60] Nevertheless, it is important to highlight that, in these segregated composite systems, the chain mobility of the bulk of the polymer micropellets remains largely unaffected by the CNTs in EM-processed composites. The disruption of polymer chain movement occurs predominantly at the CNT interphase region between the micropellets.

Additionally, the crystallization enthalpy (ΔH_c) of the EM-processed TPNCs increased by 10%, whereas the hot-pressed TPNCs showed only a 3% increase compared to pure PP. The percentage of crystallinity, x_{c_1}, of PP increased by more than 2-fold upon the addition of 0.5 wt % of CNTs. Notably, for the EM-processed TPNCs, the percentage of crystallinity increased by more than 169%, while hot-pressed TPNCs showed a slightly less 148% increment. Research indicates that incorporating CNTs changes the morphology of PP spherulites. Specifically, there may be an increase in the quantity of PP spherulites along with a reduction in their size, suggesting an improvement in the crystallization efficiency of PP. Grady et al.[63] reported a 2% increase in the crystallinity of a polypropylene grade by adding 1.8 wt % of SWNTs under nonisothermal crystallization. Mertens and Senthilvelan[64] reported that the crystallinity of CNT/PP nanocomposites increased from 47.7 to 52.5% as the CNT content rose from 0 to 1 wt % due to a CNT nucleating effect. Additionally, Alharthi,[65] research revealed an important discovery about LDPE/MWCNT nanocomposites. The study showed that exposing such nanocomposites to microwave radiation for short durations, i.e., no longer than 5 min, caused chain scission in the polymer chains. This process shortens and reorganizes the chains within the polymer matrix, resulting in a subtle but noteworthy increase in crystallinity. Conversely, long irradiation exposure resulted in significant degradation, even within the crystalline regions, and facilitated cross-linking formation due to free radicals in amorphous polymer chains, leading to a 3% reduction in crystallinity. We observed a similar crystalline behavior in the TPNCs when processed with electromagnetic radiation for approximately 3 min, which showed a marked increase in crystallinity compared to those processed via hot pressing for 6 min.

3.5. Mechanical Properties. The average values of Young's modulus, tensile strength, and elongation-at-break obtained from tensile testing for the different TPNCs are shown in Figure 14, along with their respective 95% confidence interval error bars indicating their variability. A summary of the average tensile data and their variability for the EM-processed and the hot-pressed TPNCs are also respectively presented in Tables 3 and 4. The Young's modulus showed a significant improvement with an increasing CNT content in both TPNC systems, except for the 3 wt % CNT-loaded TPNCs. For instance, the modulus of the TPNCs containing 1.5 wt % CNT was measured at 1.656 ± 0.102 GPa for the EM-processed TPNCs and at 1.424 ± 0.059 GPa for the conventionally processed ones. These values represent a substantial increase of 50 and 30% compared to the modulus of the host PP matrix (i.e., 1.115 ± 0.080 GPa), respectively. However, when the CNT loading increased to 3 wt %, the modulus significantly decreased. The reasons for such a stiffness deterioration at 3 wt % are unclear as it may be caused by multiple factors including the possible excessive heat generated by the microwave processing at higher CNT loadings, CNT agglomeration,

https://doi.org/10.1021/acsomega.4c07372
ACS Omega 2024, 9, 48546−48562

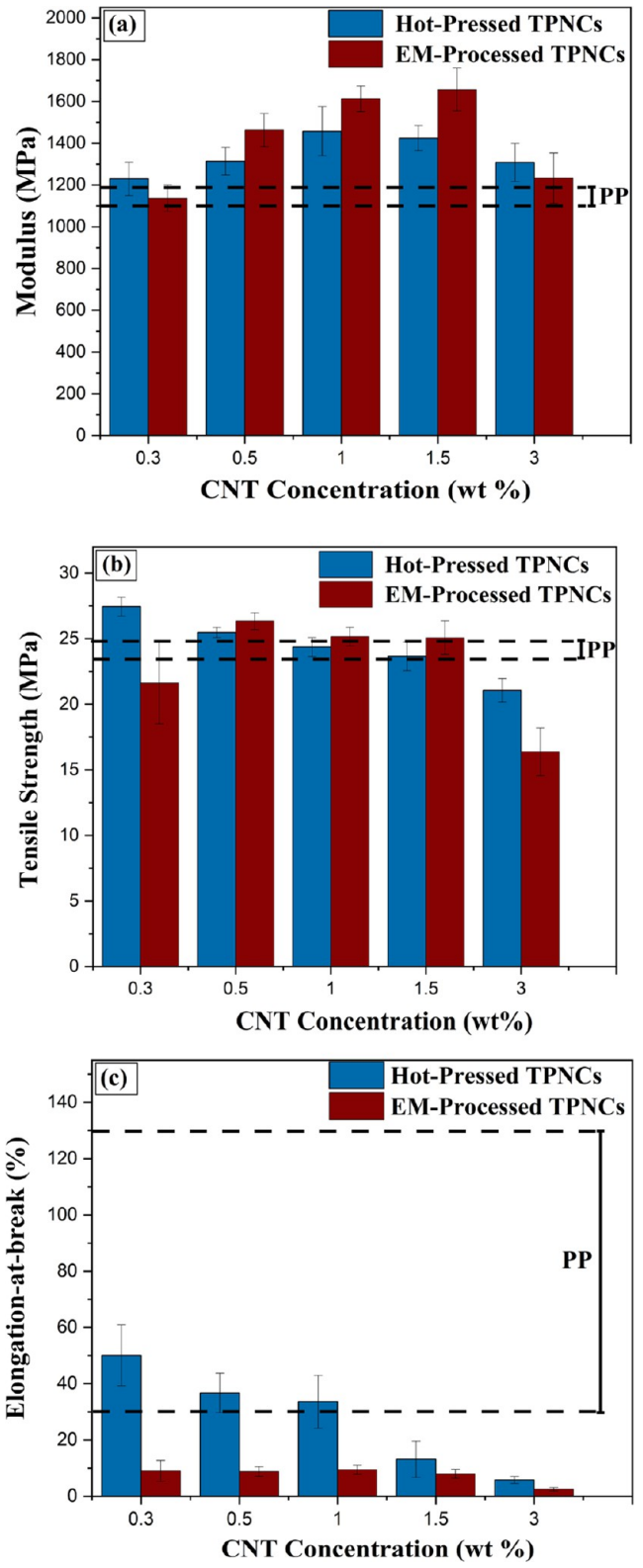

Figure 14. Tensile mechanical properties of the TPNCs as functions of CNT concentration (wt %). (a) Young's modulus, (b) tensile strength, and (c) elongation-at-break. The dotted lines represent PP pristine matrix properties error ranges, and the error ranges and bars are 95% confidence intervals.

interfacial effects, etc. Nevertheless, the effect seems to be similar for both processing methods, which makes agglomeration of CNTs at higher loadings the most feasible explanation,

Table 3. Average Tensile Testing Results for the EM-Processed TPNCs and the PP Matrix[a]

formulation	modulus (GPa)	tensile strength (MPa)	elongation-at-break (%)
PP	1.120 ± 0.080	24.32 ± 0.86	80.83 ± 51.57
0.3% CNT/PP	1.140 ± 0.060	21.63 ± 3.12	9.00 ± 3.70
0.5% CNT/PP	1.460 ± 0.070	26.33 ± 0.64	8.82 ± 1.67
1.0% CNT/PP	1.610 ± 0.060	25.15 ± 0.70	9.42 ± 1.61
1.5% CNT/PP	1.660 ± 0.100	25.07 ± 1.29	7.96 ± 1.54
3% CNT/PP	1.230 ± 0.120	16.37 ± 1.83	2.52 ± 0.62

[a]Variability values are 95% confidence intervals.

Table 4. Average Tensile Testing Results for the Hot-Pressed TPNCs and the PP Matrix[a]

formulation	modulus (GPa)	tensile strength (MPa)	elongation-at-break (%)
PP	1.120 ± 0.080	24.32 ± 0.86	80.83 ± 51.57
0.3% CNT/PP	1.230 ± 0.07	27.45 ± 0.72	50.11 ± 10.83
0.5% CNT/PP	1.314 ± 0.067	25.46 ± 0.39	36.68 ± 7.02
1.0% CNT/PP	1.457 ± 0.117	24.36 ± 0.72	33.58 ± 9.36
1.5% CNT/PP	1.425 ± 0.059	23.44 ± 1.04	13.13 ± 6.46
3% CNT/PP	1.310 ± 0.091	21.07 ± 0.89	5.84 ± 1.23

[a]Variability values are 95% confidence intervals.

since the slippage of CNTs within the CNT agglomerates and the reduced aspect ratio of the agglomerates in comparison to individual CNTs, may explain their softer behavior.[66] Furthermore, the existence of voids and imperfect CNT−matrix contact features at 3 wt % observed by SEM in Figure 7a as well as some degree of CNT pull-out detected may be indicators of a weak interfacial bonding. This weak bonding and voids lead to inefficient load transfer from the polymer to the soft CNTs interphase, which overall yields a more compliant and weaker material.[66] Despite these results at 3 wt %, the EM-processed TPNCs at lower concentrations, such as those at 1.5 wt %, seem to be benefited by potential CNT−matrix stronger interactions induced by the microwaves and/or crystallization effects as these TPNCs displayed a modulus of elasticity ∼20% higher than that of the hot-pressed TPNCs.

The tensile strength of both TPNC types displayed insignificant differences concerning the pure PP matrix at most CNT loadings, as shown in Figure 14b and Tables 3 and 4. Interestingly, however, at 0.5 wt %, the EM-processed TPNCs displayed a significantly 10% higher tensile strength with respect to the matrix. Remarkably, the incorporation of CNTs at a minimal loading of just 0.5 wt % led to enhancements in the mechanical properties of the TPNCs. This improvement can be attributed to the effective compatibilization of disentangled CNTs within the PP matrix or even chemical interactions that are beneficial at those small CNT contents. CNT reduces the barrier to PP chain alignment, resulting in a more advantageous extended chain conformation.[59] This conformation enhances stress transfer between the polymer and CNT, potentially improving the mechanical properties of the TPNCs.[59] Three types of interactions may contribute to this effect: polymer−nanotube

https://doi.org/10.1021/acsomega.4c07372
ACS Omega 2024, 9, 48546−48562

interaction, nanotube−nanotube interaction, and intrapolymer interactions within the polymer−CNT system.[59] However, as shown in Figure 14b, tensile strength starts to decrease at higher loading of CNTs (e.g., 3 wt %). The observed behavior in tensile strength at different CNT loadings aligns with the trends discussed for modulus, particularly in relation to the dispersion and agglomeration of CNTs. When CNTs agglomerate, which is more likely at higher concentrations, they lose their individual reinforcing capability, as the agglomerates exhibit a reduced aspect ratio compared to that of the individual nanotubes and behave like flaws.[66] This leads to less effective load transfer and introduces points of weakness in the matrix. Thus, the higher tensile strength observed in the EM-processed TPNCs suggests additional factors at play. Vazquez et al. highlighted that microwaves used for chemical functionalization of CNTs in the absence of solvents might activate the reactivity of CNTs, permitting their modification through new kinds of CNT−CNT and polymer−CNT reactions.[25] Such functional groups and reactions could enhance the interaction between CNTs and the polymer matrix and, as a result, their matrix−CNT load transfer.

The only TPNC property significantly affected by the incorporation of CNT was the ductility of the TPNCs. The addition of CNTs affected the TPNCs produced by both methods, and the deteriorating effect increased with the CNT loading. This effect, though, was more pronounced in the EM-processed TPNCs than in the hot-pressed TPNCs. This is likely a multicausal result, including the wide variability of the ductility of the PP grade utilized, which is a rotational molding grade with quite variable elongation-at-break. In addition, the effect of the microvoids formed during the EM melt processing (as displayed in Figure 7 and discussed in the microstructure section) may have an impact on the ductility. Moreover, while the α phase enhances stiffness, it can reduce ductility compared to the β phase.[51] The ductility of the TPNCs was statistically the same at 1.5 wt %, which means that at this "optimal" CNT loading the TPNCs maintained a balance between the elastic and ultimate properties.

As previously shown, DSC and XRD confirmed that the presence of CNTs and the microwave processing itself influences the degree of crystallinity and crystal phase of the TPNCs, which has a direct impact on the mechanical properties of the TPNCs. It is well known that crystal properties such as degree of crystallinity, spherulite size, and crystallite morphology influence the mechanical properties of semicrystalline polymers.[67] Moreover, the nucleating ability of CNTs significantly reduces the spherulite diameter and suppresses the formation of β-form crystals, even at a low loading of 0.5 wt %. Despite the relatively small proportion of β-form crystallites in neat PP, this alteration is substantial enough to account for the notable improvement in modulus and the considerable ductility reduction observed in the EM-processed TPNCs. The α phase is characterized by a more tightly packed crystal structure, contributing to higher tensile strength and stiffness, but lower ductility than the β phase.[62] Chopra et al. highlighted that the improvement in the mechanical performance of materials treated with microwave can be attributed to instantaneous local heating, which promotes chain mobility in virgin polymers, leading to the formation of smaller crystallites upon cooling. The reduction in crystallite size not only increases the strength but also the toughness of the material.[68] Thus, crystal transformations from the β phase to the α phase and the increase in crystallinity content in the TPNCs induced by the EM processing are partly responsible for the effect on the mechanical properties hereby reported.

Finally, as discussed in Figures 7 and 8, the notoriously different interphase features between the EM-processed and the conventionally processed TPNCs may have also directly impacted the mechanical properties. According to Liu et al.,[69] the interaction between the CNTs and the polymer chains leads to a microstructural development in the vicinity of CNTs that is different from that in the polymer matrix, resulting in a polymeric interphase with properties different from the bulk polymer.[69] Polymer chains near the CNT surface may undergo different crystallization processes (e.g., nucleation, different phases, etc.) directly affecting the properties of their TPNCs, like stiffness, permeability, and sometimes even strength.[69] We presume that the long and linear CNT interphase of the EM-processed TPNCs may also lead to other nucleation effects such as the formation of an additional polymeric interphase in the form of a transcrystalline layer, which may contribute to the higher TPNC stiffness.

4. CONCLUSIONS

This study demonstrates that electromagnetic (EM) melt processing of nanoformulated thermoplastics is possible to the point of being able to "synthesize" or process thermoplastic polymer nanocomposites (TPNCs) from their constituents. This is conceivable by setting up a multiscale structured network of EM-susceptible nanoparticles on the surface of thermoplastic micropellets or domains with an electrical dimension that enables electromagnetic coupling with the EM waves. In virtue of the impedance characteristics of such a network, heat may be generated from the network of nanoparticles (due to complex dissipative mechanisms) to the point of melting the domains and deforming them viscoelastically into segregated nanocomposite structures. Such multiscale structures retain a great deal of the initial nanoparticles' network yielding advanced combinations of transport and mechanical properties in the TPNCs. By controlling or selecting materials and processing parameters, this method allows for the tailoring of microstructural features, which is well-known as "structuring" in materials processing. Thus, in this study, TPNCs with segregated structures were prepared with graphitic carbon nanotubes (NC7000) in a polypropylene matrix (Matrix Polymers Revolve PP46). The proposed EM processing was systematically compared to conventional processing, and the properties and microstructures of the TPNCs were contrasted. Our study found that EM processing significantly enhances the electrical conductivity of TPNCs when compared to hot-pressed TPNCs. EM-processed TPNCs exhibited a significantly lower percolation threshold of less than 0.1 vol %, i.e., ten times smaller than that of hot-pressed TPNCs. Interestingly, at only 1 wt %, the EM-processed TPNCs displayed electrical conductivities at least 8 orders of magnitude greater than their corresponding hot-pressed counterparts. Furthermore, the EM-processed TPNCs retained a well-defined microstructural network due to the localized EM heating, and their microstructure showed a defined and thin CNT interphase that formed a segregated but electrically percolated morphology. In contrast, the hot-pressed TPNCs showed a larger network distortion, with a diffused and spread CNT interphase. Furthermore, thermal analysis revealed that EM processing led to more crystalline TPNCs than conventional

https://doi.org/10.1021/acsomega.4c07372
ACS Omega 2024, 9, 48546−48562

processing. Very significantly, X-ray diffraction analysis of the TPNCs indicated that microwave processing also favored the formation of the α crystal phase, which is stiffer and less ductile than the formed β phase in the pristine PP. This was consistent with the tensile properties of the TPNCs, as the EM-processed TPNCs exhibited statistically significant higher stiffness and slightly higher strength than the hot-pressed TPNCs at corresponding compositions. We theorize that localized heating may have not only produced infiltration of the polymeric chains into the CNT interphase and the CNTs themselves but also EM-induced matrix−CNT interfacial interactions or even chemical bonding that may have affected positively or negatively the matrix−CNT stress transfer depending on the CNT concentration. The ductility, though, of the EM-processed TPNCs was significantly less than that of the hot-pressed TPNCs, which is believed to be a multicausal phenomenon, that includes crystallization effects due to the formation of the less ductile α phase and a higher percentage of crystallinity, to the extremely variable ductility of the rotational molding PP grade, and the formation of local microvoids during the inductive irradiation step, as supported by SEM micrographs. Therefore, this study establishes the relevance and importance of electromagnetic melt-processing of TPNCs as a novel and viable methodology to achieve breakthrough multiscale structuring in segregated TPNCs for tailored and advanced functional properties. The higher transport properties of the EM-processed TPNCs may be suitable for applications in defense, electronics, smart devices, photonics, phononics, sensors, actuators, dielectrics, metamaterials, robotics, and even biomedicine. Further research and optimization of material and processing parameters could lead to even greater improvements in the performance and applicability of this unconventional and unique material processing methodology and to cutting-edge functional materials produced thereby. Thus, future studies must focus on critical material and processing parameters, such as polymer type, polymer particle size effect, aspect ratio of the nanomaterials, and nanomaterial type, as well as microwave processing power, time, and premixing conditions.

■ ASSOCIATED CONTENT

Supporting Information

The Supporting Information is available free of charge at https://pubs.acs.org/doi/10.1021/acsomega.4c07372.

Video of the electromagnetic melt processing of a specimen taking place inside a microwave oven (AVI)

■ AUTHOR INFORMATION

Corresponding Author

Byron S. Villacorta − *Department of Chemical Engineering, University of Mississippi School of Engineering, University, Mississippi 38677, United States; Center for Graphene Research and Innovation, University of Mississippi School of Engineering, University, Mississippi 38677, United States; School of Mechanical and Mining Engineering, University of Queensland School of Engineering, Saint Lucia, QLD 4072, Australia;* orcid.org/0000-0002-9252-2476; Email: bsvillac@olemiss.edu

Authors

Madara Mohoppu − *Department of Chemical Engineering, University of Mississippi School of Engineering, University, Mississippi 38677, United States; Center for Graphene Research and Innovation, University of Mississippi School of Engineering, University, Mississippi 38677, United States*

Utsab Ayan − *Department of Chemical Engineering, University of Mississippi School of Engineering, University, Mississippi 38677, United States; Center for Graphene Research and Innovation, University of Mississippi School of Engineering, University, Mississippi 38677, United States*

Jacob Schwartz − *Department of Chemical Engineering, University of Mississippi School of Engineering, University, Mississippi 38677, United States*

Ahmed Al-Ostaz − *Center for Graphene Research and Innovation and Department of Civil Engineering, University of Mississippi School of Engineering, University, Mississippi 38677, United States*

Mine G. Ucak-Astarlioglu − *U.S. Army Engineer Research and Development Center, Geotechnical and Structures Laboratory, Vicksburg, Mississippi 39180-6199, United States;* orcid.org/0000-0003-4186-1707

Complete contact information is available at: https://pubs.acs.org/10.1021/acsomega.4c07372

Notes

The authors declare no competing financial interest.

■ ACKNOWLEDGMENTS

The work described in this document was conducted at the Center for Graphene Research and Innovation and the Department of Chemical Engineering at the University of Mississippi. The authors acknowledge the support provided by the U.S. Army Engineer Research and Development Center (ERDC) and the Military Engineering Research and Development Area under contract W912HZ21C0040. Permission to publish was granted by the ERDC Geotechnical and Structures Laboratory.

■ REFERENCES

(1) de Leon, A. C.; Chen, Q.; Palaganas, N. B.; Palaganas, J. O.; Manapat, J.; Advincula, R. C. High Performance Polymer Nanocomposites for Additive Manufacturing Applications. *React. Funct. Polym.* **2016**, *103*, 141−155.

(2) Hassan, T.; Salam, A.; Khan, A.; Khan, S. U.; Khanzada, H.; Wasim, M.; Khan, M. Q.; Kim, I. S. Functional Nanocomposites and Their Potential Applications: A Review. *J. Polym. Res.* **2021**, *28*, No. 36.

(3) Villacorta, B.; Ayan, U.; Mohoppu, M.; Kattel, B.; Hutchcraft, E.; Ucak-Astarlioglu, M.; Al-Ostaz, A. Flexible Polyethylene Matrix Carbon-Based Nanocomposites for Electromagnetic Compatibility. *ACS Appl. Electron. Mater.* **2024**, *6*, 5379−5390.

(4) Fu, S.; Sun, Z.; Huang, P.; Li, Y.; Hu, N. Some Basic Aspects of Polymer Nanocomposites: A Critical Review. *Nano Mater. Sci.* **2019**, *1* (1), 2−30.

(5) Fakirov, S. Polymer Nanocomposites: Why Their Mechanical Performance Does Not Justify the Expectation and a Possible Solution to the Problem? *Express Polym. Lett.* **2020**, *14*, 436−466.

(6) Zare, Y. Study of Nanoparticles Aggregation/Agglomeration in Polymer Particulate Nanocomposites by Mechanical Properties. *Composites, Part A* **2016**, *84*, 158−164.

(7) Huang, C.; Qian, X.; Yang, R. Thermal Conductivity of Polymers and Polymer Nanocomposites. *Mater. Sci. Eng., R* **2018**, *132*, 1−22.

(8) Smith, J. S.; Bedrov, D.; Smith, G. D. A Molecular Dynamics Simulation Study of Nanoparticle Interactions in a Model Polymer-Nanoparticle Composite. *Compos. Sci. Technol.* **2003**, *63* (11), 1599−1605.

(9) Qiao, R.; Brinson, L. C. Simulation of Interphase Percolation and Gradients in Polymer Nanocomposites. *Compos. Sci. Technol.* **2009**, *69* (3−4), 491−499.
(10) Ma, P. C.; Siddiqui, N. A.; Marom, G.; Kim, J. K. Dispersion and Functionalization of Carbon Nanotubes for Polymer-Based Nanocomposites: A Review. *Composites, Part A* **2010**, *41* (10), 1345−1367.
(11) Gkikas, G.; Barkoula, N. M.; Paipetis, A. S. Effect of Dispersion Conditions on the Thermo-Mechanical and Toughness Properties of Multi Walled Carbon Nanotubes-Reinforced Epoxy. *Composites, Part B* **2012**, *43* (6), 2697−2705.
(12) Du, H.; Spratford, S.; Shan, J. W.; Weng, G. J. Experimental and Theoretical Study of the Evolution of Fluid-Suspended Graphene Morphology Driven by an Applied Electric Field and the Attainment of Ultra-Low Percolation Threshold in Graphene-Polymer Nanocomposites. *Compos. Sci. Technol.* **2020**, *199*, No. 108315.
(13) Oseli, A.; Tomković, T.; Hatzikiriakos, S. G.; Vesel, A.; Arzenšek, M.; Rojac, T.; Mihelčič, M.; Perše, L. S. Carbon Nanotube Network Formation and Configuration/Morphology on Reinforcing and Conductive Performance of Polymer-Based Nanocomposites. *Compos. Sci. Technol.* **2023**, *237*, No. 110010.
(14) Mousavi, S. R.; Estaji, S.; Kiaei, H.; Mansourian-Tabaei, M.; Nouranian, S.; Jafari, S. H.; Ruckdäschel, H.; Arjmand, M.; Khonakdar, H. A. A Review of Electrical and Thermal Conductivities of Epoxy Resin Systems Reinforced with Carbon Nanotubes and Graphene-Based Nanoparticles. *Polym. Test.* **2022**, *112*, No. 107645.
(15) Tadmor, Z.; Gogos, C. G. *Principles of Polymer Processing*; John Wiley & Sons, 2013.
(16) Villacorta, B. *Electromagnetic Shielding of Carbon Modifiers/Polyethylene Composites* 2014.
(17) Sgriccia, N.; Hawley, M. C. Thermal, Morphological, and Electrical Characterization of Microwave Processed Natural Fiber Composites. *Compos. Sci. Technol.* **2007**, *67* (9), 1986−1991.
(18) Chaowasakoo, T.; Sombatsompop, N. Mechanical and Morphological Properties of Fly Ash/Epoxy Composites Using Conventional Thermal and Microwave Curing Methods. *Compos. Sci. Technol.* **2007**, *67* (11−12), 2282−2291.
(19) Zhou, L.; Tian, Y.; Xu, P.; Wei, H.; Li, Y.; Peng, H. X.; Qin, F. Effect of the Selective Localization of Carbon Nanotubes and Phase Domain in Immiscible Blends on Tunable Microwave Dielectric Properties. *Compos. Sci. Technol.* **2021**, *213*, No. 108919.
(20) Kasap, S. O. *Electronic Materials and Devices*; McGraw-Hill: New York, 2006.
(21) Mishra, R. R.; Sharma, A. K. Microwave-Material Interaction Phenomena: Heating Mechanisms, Challenges and Opportunities in Material Processing. *Composites, Part A* **2016**, *81*, 78−97.
(22) Mishra, R. R.; Sharma, A. K. Composites: Part A Microwave − Material Interaction Phenomena: Heating Mechanisms, Challenges and Opportunities in Material Processing. *Composites, Part A* **2016**, *81*, 78−97.
(23) Pozar, D. M. *Microwave Engineering*; Wiley: Hoboken, NJ, USA, 2005.
(24) Al-saleh, M. H.; Sundararaj, U. Electromagnetic Interference Shielding Mechanisms of CNT/Polymer Composites. *Carbon* **2009**, *47* (7), 1738−1746.
(25) Vázquez, E.; Prato, M. Carbon Nanotubes and Microwaves. *ACS Nano* **2009**, *3* (12), 3819−3824.
(26) Wu, T.; Pan, Y.; Liu, E.; Li, L. Carbon Nanotube/Polypropylene Composite Particles for Microwave Welding. *J. Appl. Polym. Sci.* **2012**, *126* (S2), E283−E289.
(27) Xu, D.; Chen, W.; Liu, P. Enhanced Electromagnetic Interference Shielding and Mechanical Properties of Segregated Polymer/Carbon Nanotube Composite via Selective Microwave Sintering. *Compos. Sci. Technol.* **2020**, *199*, No. 108355.
(28) Sweeney, C. B.; Lackey, B. A.; Pospisil, M. J.; Achee, T. C.; Hicks, V. K.; Moran, A. G.; Teipel, B. R.; Saed, M. A.; Green, M. J. Welding of 3D-Printed Carbon Nanotube−Polymer Composites by Locally Induced Microwave Heating. *Sci. Adv.* **2017**, *3* (6), No. e1700262.
(29) Naik, T. P.; Singh, I.; Sharma, A. K. Processing of Polymer Matrix Composites Using Microwave Energy: A Review. *Composites, Part A* **2022**, *156*, No. 106870.
(30) Odom, M. G. B.; Sweeney, C. B.; Parviz, D.; Sill, L. P.; Saed, M. A.; Green, M. J. Rapid Curing and Additive Manufacturing of Thermoset Systems Using Scanning Microwave Heating of Carbon Nanotube/Epoxy Composites. *Carbon* **2017**, *120*, 447−453.
(31) Li, Y.; Li, N.; Zhou, J.; Cheng, Q. Microwave Curing of Multidirectional Carbon Fiber Reinforced Polymer Composites. *Compos. Struct.* **2019**, *212*, 83−93.
(32) Thostenson, E. T.; Chou, T. W. Microwave Processing: Fundamentals and Applications. *Composites, Part A* **1999**, *30* (9), 1055−1071.
(33) Zhou, S.; Hawley, M. C. A Study of Microwave Reaction Rate Enhancement Effect in Adhesive Bonding of Polymers and Composites. *Compos. Struct.* **2003**, *61* (4), 303−309.
(34) Wang, C.; Chen, T.; Chang, S.; Cheng, S.; Chin, T. Strong Carbon-Nanotube-Polymer Bonding by Microwave Irradiation. *Adv. Funct. Mater.* **2007**, *17* (12), 1979−1983.
(35) Feng, D.; Xu, D.; Wang, Q.; Liu, P. Highly Stretchable Electromagnetic Interference (EMI) Shielding Segregated Polyurethane/Carbon Nanotube Composites Fabricated by Microwave Selective Sintering. *J. Mater. Chem. C* **2019**, *7* (26), 7938−7946.
(36) Feng, D.; Liu, P.; Wang, Q. Carbon Nanotubes in Microwave-Assisted Foaming and Sinter Molding of High Performance Polyetherimide Bead Foam Products. *Mater. Sci. Eng., B* **2020**, *262*, No. 114727.
(37) Villacorta, B.; Zhu, Z.; Truss, R.; Larsen, A.; Solomon, G. Method for Fabricating Carbon Nanoparticle Polymer Matrix Composites Using Electromagnetic Irradiation 2023 https://patentimages.storage.googleapis.com/ca/61/13/08aadf441e26ea/US20230137272A1.pdf.
(38) Campo, N.; Visco, A. M. Incorporation of Carbon Nanotubes into Ultra High Molecular Weight Polyethylene by High Energy Ball Milling. *Int. J. Polym. Anal. Charact.* **2010**, *15* (7), 438−449.
(39) Paul, C. R.; Scully, R. C.; Steffka, M. A. *Introduction to Electromagnetic Compatibility*; John Wiley & Sons, 2022.
(40) Lyu, H.; Gao, B.; He, F.; Ding, C.; Tang, J.; Crittenden, J. C. Ball-Milled Carbon Nanomaterials for Energy and Environmental Applications. *ACS Sustainable Chem. Eng.* **2017**, *5* (11), 9568−9585.
(41) Krause, B.; Villmow, T.; Boldt, R.; Mende, M.; Petzold, G.; Pötschke, P. Influence of Dry Grinding in a Ball Mill on the Length of Multiwalled Carbon Nanotubes and Their Dispersion and Percolation Behaviour in Melt Mixed Polycarbonate Composites. *Compos. Sci. Technol.* **2011**, *71* (8), 1145−1153.
(42) Untereker, D.; Lyu, S.; Schley, J.; Martinez, G.; Lohstreter, L. Maximum Conductivity of Packed Nanoparticles and Their Polymer Composites. *ACS Appl. Mater. Interfaces* **2009**, *1* (1), 97−101.
(43) Ma, P. C.; Liu, M. Y.; Zhang, H.; Wang, S. Q.; Wang, R.; Wang, K.; Wong, Y. K.; Tang, B. Z.; Hong, S. H.; Paik, K. W.; Kim, J. K. Enhanced Electrical Conductivity of Nanocomposites Containing Hybrid Fillers of Carbon Nanotubes and Carbon Black. *ACS Appl. Mater. Interfaces* **2009**, *1* (5), 1090−1096.
(44) Li, J.; Ma, P. C.; Chow, W. S.; To, C. K.; Tang, B. Z.; Kim, J. K. Correlations between Percolation Threshold, Dispersion State, and Aspect Ratio of Carbon Nanotubes. *Adv. Funct. Mater.* **2007**, *17* (16), 3207−3215.
(45) Yu, Y.; Song, S.; Bu, Z. Influence of Filler Waviness and Aspect Ratio on the Percolation Threshold of Carbon Nanomaterials Reinforced Polymer Nanocomposites. *J. Mater. Sci.* **2013**, *48*, 5727−5732.
(46) Wang, J.; Kazemi, Y.; Wang, S.; Hamidinejad, M.; Mahmud, M. B.; Pötschke, P.; Park, C. B. Enhancing the Electrical Conductivity of PP/CNT Nanocomposites through Crystal-Induced Volume Exclusion Effect with a Slow Cooling Rate. *Composites, Part B* **2020**, *183*, No. 107663.
(47) Coppola, B.; Di Maio, L.; Incarnato, L.; Tulliani, J. M. Preparation and Characterization of Polypropylene/Carbon Nano-

https://doi.org/10.1021/acsomega.4c07372
ACS Omega 2024, 9, 48546−48562

tubes (PP/CNTs) Nanocomposites as Potential Strain Gauges for Structural Health Monitoring. *Nanomaterials* **2020**, *10* (4), No. 814.
(48) Gaikwad, S. D.; Goyal, R. K. Effect of Manufacturing Processes on Percolation Threshold and Electrical Conductivity of Polymer/Multi Layers Graphene Nanocomposites. *Diamond Relat. Mater.* **2018**, *85*, 13−17.
(49) Wang, Q.; Wang, X.; Fang, P.; Wang, D.; Dai, Y.; Wang, S.; Liew, M.; Xu, Z. Crystallization Behavior of Polypropylene/Polyamide 6/Montmorillonite Nanocomposites. *Polym. Int.* **2010**, *59*, 1303−1309.
(50) Jafari, M.; Vaezzadeh, M.; Noroozizadeh, S. Thermal Stability of α Phase of Titanium by Using X-Ray Diffraction. *Metall. Mater. Trans. A* **2010**, *41* (13), 3287−3290.
(51) Karger-Kocsis, J.; Varga, J. Effects of?-? Transformation on the Static and Dynamic Tensile Behavior of Isotactic Polypropylene. *J. Appl. Polym. Sci.* **1996**, *62* (2), 291−300.
(52) Kalaitzidou, K.; Fukushima, H.; Askeland, P.; Drzal, L. T. The Nucleating Effect of Exfoliated Graphite Nanoplatelets and Their Influence on the Crystal Structure and Electrical Conductivity of Polypropylene Nanocomposites. *J. Mater. Sci.* **2008**, *43* (8), 2895−2907.
(53) Tordjeman, P.; Robert, C.; Marin, G.; Gerard, P. The Effect of α, β Crystalline Structure on the Mechanical Properties of Polypropylene. *Eur. Phys. J. E* **2001**, *4* (4), 459−465.
(54) Jeon, K.; Warnock, S.; Ruiz-Orta, C.; Kismarahardja, A.; Brooks, J.; Alamo, R. G. Role of Matrix Crystallinity in Carbon Nanotube Dispersion and Electrical Conductivity of IPP-Based Nanocomposites. *J. Polym. Sci., Part B:Polym. Phys.* **2010**, *48* (19), 2084−2096.
(55) Yang, Z.; Peng, H.; Wang, W.; Liu, T. Crystallization Behavior of Poly(ε-Caprolactone)/Layered Double Hydroxide Nanocomposites. *J. Appl. Polym. Sci.* **2010**, *116* (5), 2658−2667.
(56) Cho, K.; Li, F.; Choi, J. Crystallization and Melting Behavior of Polypropylene and Maleated Polypropylene Blends. *Polymer* **1999**, *40*, 1719−1729.
(57) Taylor, P.; Lu, S.; He, M.; Lu, S.; Zhou, Z.; Yu, J.; Li, F.; He, M. Study on the Influence of Crystal Structures on the Performance of Low-Melting Polyamide 6. *Polym.-Plast. Technol. Eng.* **2014**, *52*, 157−162, DOI: 10.1080/03602559.2012.734360.
(58) Ayan, U.; Nouranian, S.; Majdoub, M.; Al-ostaz, A.; Ucak-astarlioglu, M. G.; Villacorta, B. S. Supertoughened Polylactic Acid/Polybutylene Adipate Terephthalate Blends Compatibilized with Ethylene-Methyl Acrylate-Glycidyl Methacrylate: Morphology and Mechanical Properties by the Response Surface Methodology. *ACS Appl. Mater. Interfaces* **2024**, *16*, 26833−26848.
(59) Bikiaris, D. Microstructure and Properties of Polypropylene/Carbon Nanotube Nanocomposites. *Materials* **2010**, *3*, 2884−2946.
(60) Lin, Z. I.; Lou, C. W.; Pan, Y. J.; Hsieh, C. T.; Huang, C. L.; Huang, C. H.; Chen, Y. S.; Lin, J. H. The Effects of MWCNT Length on the Mechanical, Crystallization and Electromagnetic Interference Shielding Effectiveness of PP/MWCNT Composites. *J. Polym. Res.* **2017**, *24*, No. 32.
(61) Ondreas, F.; Lepcio, P.; Zboncak, M.; Zarybnicka, K.; Govaert, L. E.; Jancar, J. Effect of Nanoparticle Organization on Molecular Mobility and Mechanical Properties of Polymer Nanocomposites. *Macromolecules* **2019**, *52* (16), 6250−6259.
(62) Xu, D.; Wang, Z. Role of Multi-Wall Carbon Nanotube Network in Composites to Crystallization of Isotactic Polypropylene Matrix. *Polymer* **2008**, *49* (1), 330−338.
(63) Probst, O.; Moore, E. M.; Resasco, D. E.; Grady, B. P. Nucleation of Polyvinyl Alcohol Crystallization by Single-Walled Carbon Nanotubes. *Polymer* **2004**, *45* (13), 4437−4443.
(64) Mertens, A. J.; Senthilvelan, S. Mechanical and Tribological Properties of Carbon Nanotube Reinforced Polypropylene Composites. *Proc. Inst. Mech. Eng., Part L* **2018**, *232* (8), 669−680.
(65) Al-harthi, M. A. Influence of Applying Microwave Radiation on the LDPE/MWCNTs Nanocomposite. *Polym. Compos.* **2014**, *35* (10), 2036−2042.
(66) Bhuiyan, M. A.; Pucha, R. V.; Worthy, J.; Karevan, M.; Kalaitzidou, K. Defining the Lower and Upper Limit of the Effective Modulus of CNT/Polypropylene Composites through Integration of Modeling and Experiments. *Compos. Struct.* **2013**, *95*, 80−87.
(67) Yetgin, S. H. Effect of Multi Walled Carbon Nanotube on Mechanical, Thermal and Rheological Properties of Polypropylene. *J. Mater. Res. Technol.* **2019**, *8* (5), 4725−4735.
(68) Chopra, S.; Pande, K.; Kelkar, A.; et al. Understanding the Structural Changes, Interfacial Mechanisms, and Mechanical Properties of Polymer/MWCNT Nanocomposites after Microwave Treatment. *Polym. Compos.* **2023**, 1−14, DOI: 10.1002/pc.28010.
(69) Liu, Y.; Kumar, S. Polymer_Carbon Nanotube Nano Composite Fibers−A Review. *ACS Appl. Mater. Interfaces* **2014**, *6*, 6069−6087.

https://doi.org/10.1021/acsomega.4c07372
ACS Omega 2024, 9, 48546−48562